Delft University of Technology

Studying the impact of phase behavior in the morphology of molecular dynamics models of bitumen

Assaf, Eli I.; Liu, Xueyan; Lin, Peng; Erkens, Sandra; Nahar, Sayeda; Mensink, Liz I.S.

DOI
10.1016/j.matdes.2023.111943

Publication date
2023

Document Version
Final published version

Published in
Materials and Design

Citation (APA)
Assaf, E. I., Liu, X., Lin, P., Erkens, S., Nahar, S., & Mensink, L. I. S. (2023). Studying the impact of phase behavior in the morphology of molecular dynamics models of bitumen. *Materials and Design*, *230*, Article 111943. https://doi.org/10.1016/j.matdes.2023.111943

Important note
To cite this publication, please use the final published version (if applicable).
Please check the document version above.

Copyright
Other than for strictly personal use, it is not permitted to download, forward or distribute the text or part of it, without the consent of the author(s) and/or copyright holder(s), unless the work is under an open content license such as Creative Commons.

Takedown policy
Please contact us and provide details if you believe this document breaches copyrights.
We will remove access to the work immediately and investigate your claim.

This work is downloaded from Delft University of Technology.
For technical reasons the number of authors shown on this cover page is limited to a maximum of 10.

Materials & Design 230 (2023) 111943

Contents lists available at ScienceDirect

Materials & Design

journal homepage: www.elsevier.com/locate/matdes

Studying the impact of phase behavior in the morphology of molecular dynamics models of bitumen

Eli I. Assaf [a,*], Xueyan Liu [a], Peng Lin [a], Sandra Erkens [a], Sayeda Nahar [b], Liz I.S. Mensink [c]

[a] Delft University of Technology, Delft, The Netherlands
[b] Netherlands Organization for Applied Scientific Research (TNO), The Netherlands
[c] Ministry of Infrastructure and Water Management (Rijkswaterstaat), The Netherlands

HIGHLIGHTS

- Homogeneous models of bitumen undergo significant phase separation of its SARA fractions after long simulation times.
- MD models of bitumen can exhibit heterogenous morphologies resembling those of mixtures that have undergone phase separation.
- Unlike homogenous bitumen morphologies, heterogeneous models are stable and undergo negligible phase separation over time.
- More sophisticated techniques are needed to measure the physical differences between bitumen models having different morphologies.
- Phase separation in MD models of bitumen results in a lower and even distribution of energies between the atoms.

GRAPHICAL ABSTRACT

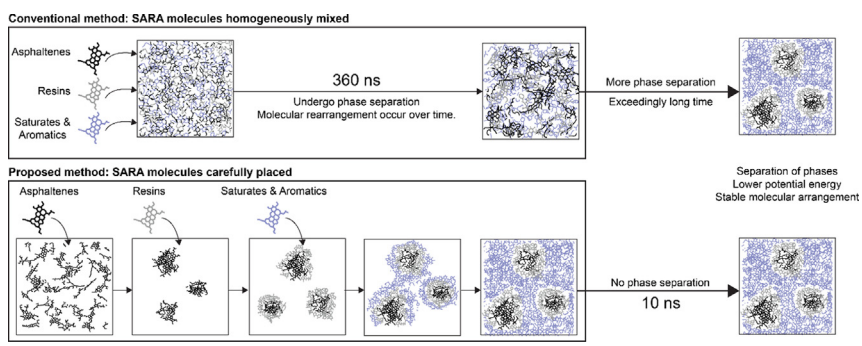

ARTICLE INFO

Article history:
Received 3 November 2022
Revised 18 March 2023
Accepted 18 April 2023
Available online 23 April 2023

Keywords:
Bitumen
Molecular dynamics
Phase separation
Morphology
Colloids

ABSTRACT

Conventional Molecular Dynamics (MD) models of bitumen are built by homogeneously mixing molecules in a volume without considering that the molecules in bitumen are known to exhibit phase behavior and form distinctive molecular arrangements. These are known to have a significant impact in the behavior of bitumen, and considering their existence is paramount in producing improved representations of bitumen using computational models. This study explores whether MD models of bitumen that are conventionally assumed to be in equilibrium can still undergo significant phase separation over considerably long simulation times. It also aims to establish a more formal pathway to build and study models with highly heterogeneous arrangements of their molecules. Moreover, it aims to evaluate whether the presence of distinct morphologies have a significant impact in numerous physical properties of bitumen. The study shows that conventional and widely used models of bitumen exhibit significant molecular rearrangements over long times (>360 ns). It also shows that building heterogeneous morphologies is possible and result in energetically favorable conformations. Moreover, it proves that studying properties regularly used to validate MD models of bitumen (e.g., density) are insufficient in assessing the impact of different morphologies; more thorough methods are required to evaluate them.

© 2023 The Author(s). Published by Elsevier Ltd. This is an open access article under the CC BY license (http://creativecommons.org/licenses/by/4.0/).

* Corresponding author.
E-mail address: e.i.assaf@tudelft.nl (E.I. Assaf).

https://doi.org/10.1016/j.matdes.2023.111943
0264-1275/© 2023 The Author(s). Published by Elsevier Ltd.
This is an open access article under the CC BY license (http://creativecommons.org/licenses/by/4.0/).

1. Introduction

Roads constitute the backbone of having a functional transport network and keeping them well-maintained and in operation is crucial for fomenting economic growth and stability. Therefore, there has always been a considerable amount of effort invested in improving the performance and durability of asphalt mixtures. To enhance their durability and performance, scientists have mostly focused on improving the mechanical and rheological properties of bitumen, as bitumen is known to strongly dictate whether the physical response of an asphalt mixture is suitable for road operations. Most of the studies performed on bituminous materials until now have focused on describing the behavior of bitumen at an engineering scale. However, recent technological development and an increased awareness for sustainability have persuaded scientists to utilize more fundamental methods to model bitumen at a molecular scale, hoping that a more thorough characterization would aid them in the design of enhanced bituminous materials.

Describing the structure of bitumen on a molecular scale has been proven to be a remarkably challenging task. The chemical composition of bitumen varies considerably depending on the source, as well as on the refining and testing methods used to produce it and characterize it, resulting in a material whose formal definition remains uncertain. Moreover, the atomic structures of most of the molecules in bitumen are currently under dispute, as bitumen is composed of millions of dissimilar organic molecules that vary significantly in aromaticity, saturation, polarity, and size[1–3]. These variations push molecules to exhibit phase behavior, which results in the formation of physically separated portions of matter that develop into complex molecular arrangements. These molecular arrangements give each bitumen a unique morphology, significantly changing the mechanical and rheological response of the material. The existence of these molecular arrangements is also known to span over several size domains, adding significant multiscale characterization challenges that are less prevalent in other materials like in many types of metals or polymers.

The use of Quantum Mechanics (QM) and Molecular Dynamics (MD) methods has aided scientists in fundamentally describing bituminous materials at a molecular scale, but computational resources limit their use to the structural elucidation of single molecules or to simulations involving the dynamics of models a few nanometers in size. Currently, scientists build atomistic models of bitumen by homogeneously mixing molecules in a simulation box without considering that the difference in aromaticity, saturation, polarity, and size between the molecules can lead to the formation of distinctive molecular arrangements. They argue that these form at a scale that is substantially larger than the one characteristic of current MD simulations and that the properties measured with current models are accurate enough to justify their implementation. However, many research papers, whose bitumen models are just a few molecules in size, already report the aggregation of molecules over the course of their simulations, raising the question on whether a conventional MD model of bitumen can undergo significant phase separation and if bituminous models built using the same molecules are equivalent and comparable despite having different molecular arrangements. Exploring the impact of phase separation can aid scientists in reproducing larger scale phenomena known to occur in bitumen and in better linking the chemical properties of a bitumen sample with its mechanical and rheological response. Moreover, formalizing the use of phase separation in computational models of bitumen can aid scientists in measuring the stability of a real bituminous mixture, as a more fundamental explanation will assist to describe why many bitumens are prone to undergo segregation and degrade over time[4].

The aim of this study focusses on exploring whether MD models of bitumen that are conventionally assumed to be in equilibrium can still undergo significant phase separation of its molecules over considerably long simulation times. It also aims to establish a more formal pathway to study molecular arrangements in these models and evaluate whether the presence of distinct morphologies have a significant impact in numerous physical properties of bitumen. To achieve this, the manuscript starts with a brief background of the research performed on bitumen to illustrate how scientists have used both experimental and computational methods to fundamentally characterize it. It then proceeds to give a description of all the methods, assumptions, and parameters used to perform the simulations of this study. The section that follows introduces two model construction methods used to successfully build models of bitumen with intentionally different morphologies. The *Conventional Method*, used by Greenfield et al[5,6] and other researchers to build models of bitumen, is used to explore whether bitumen models that are inherently homogeneous can undergo significant phase separation. The *Heterogeneous Method* is proposed specifically to build models of bitumen that have already undergone a certain degree of phase separation, whose molecular fractions are purposedly placed into clustered arrangements to produce increasingly separated molecular morphologies. It then provides details of all the quantities and techniques used to evaluate the validity and morphology of the bitumen models. Among these, there are relevant bulk properties such as density, cohesive energy density, heat capacity, thermal conductivity, and self-diffusivity constants, used to validate and compare the influence of different molecular arrangements. Additionally, there is a cluster counting algorithm that tracks the growth, size, and shape of asphaltene clusters, a nearest neighbor algorithm that assesses whether the molecules are exhibiting phase separation, and a script that tracks the local potential energies distributions in both bulk and interfacial regions within the bitumen model to assess whether the process is thermodynamically driven. The following section introduces a series of MD tests that are performed to examine the development of the quantities presented in the previous section. These tests include a considerably long *stability* run, a *heating cycle*, followed by another considerably long *stability* run. The last section focuses on presenting and discussing the findings of this study. A schematic of all the sections in this manuscript is presented in Fig. 1.

2. Background

2.1. Experimental

Experimental attempts to chemically characterize bitumen separate its molecules into distinct chemical fractions based on their solubility. The earliest attempts separated bitumen into two fractions: asphaltenes and maltenes, but since the latter were by far the most numerous, separating it into just two fractions became insufficient[7]. Corbett later separated the maltenes fraction into saturates, aromatics, and resins using an elution-adsorption liquid chromatography method with solvents of varying polarity and aromaticity[8]. This method fractionated bitumen into its so-called SARA fractions: the Saturates, Aromatics, Resins, and Asphaltenes, and has become a widely used technique to experimentally describe the chemical composition of a bitumen sample[9–11]. The Saturates are a transparent liquid composed of branched and linear aliphatic hydrocarbon chains with negligible polarity and represent 5–15% by weight of bitumen[12]. The Aromatics consist of a viscous liquid comprised of highly apolar hydrocarbons with one or more aromatic rings. They represent 30–45% by weight of bitumen. The Resins are aromatic compounds with highly polar functional groups, mostly comprised of heteroatoms like oxygen,

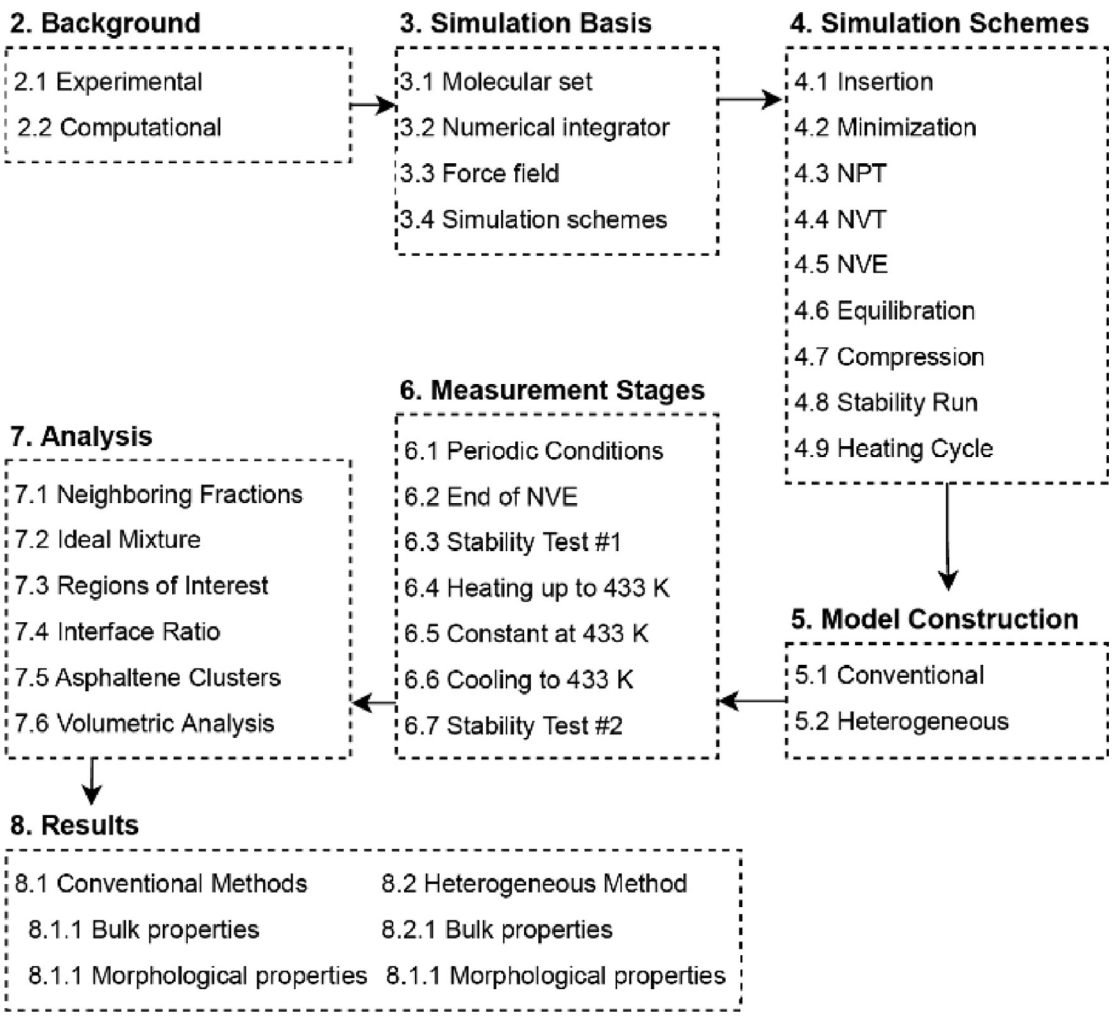

Fig. 1. Diagram depicting the different sections of this manuscript.

sulfur, or nitrogen. They represent 30–45% by weight of bitumen and consist of a black solid[13]. The Asphaltenes consist of a dark, solid-like substance composed of high molecular weight hydrocarbons with many aromatic rings and polar functional groups[14]. They represent about 5–20% by weight of bitumen and are known to give bitumen its stiffness and viscosity[15].

The ability to separate bitumen into different chemical fractions raised interest in understanding how these fractions with different solubilities interact to produce a seemingly homogeneous mixture of hydrocarbons. Rosinger and Nellesteyn were the first to raise the thought that bitumen had a delicate nanostructure comprised of a colloidal dispersion of asphaltenes in a solution of maltenes. They suggested that the asphaltenes were kept in a colloidal suspension by the action of surfactant agents present in the maltenes fraction, which would explain how two solutions with different polarities would remain together. Mieczyslaw[16] and Speight proposed that the molecules in the asphaltenes fraction exhibit phase behavior, as they appeared to agglomerate and cluster, suggesting that the physical properties of bitumen were significantly influenced by the number, shape, and how well dispersed and stable the asphaltene molecules were in the molecular arrangement of the bitumen samples. This clustering behavior of asphaltene molecules was attributed to the decrease in potential energy that two or more asphaltene molecules experienced when forming a cluster[17]. The colloidal structure of bitumen was suggested to be composed of asphaltene clusters of different shapes and sizes surrounded by a shell of stabilizing resins, which in turn are dispersed in a solution of saturates and aromatics.

Further work by Pfeiffer and Saal suggested that the arrangement and interaction of these colloidal particles (in the nanometer scale) can interact to form even larger arrangements (well within the micrometer range), which they identified as *sol* and the *gel* bitumens. The difference between these morphologies would have a significant impact in the rheological properties and behavior of bitumen[2]. In the sol bitumens, the low content of asphaltenes were thought to result in non-interacting asphaltene clusters that were well dispersed by a (relatively) high number of resins, which functioned as surfactants to keep them in a stable colloidal suspension. Sol bitumens exhibited high temperature susceptibility, high ductility, and lower aging rates[18]. In gel bitumens, the high content of asphaltenes was believed to result in an interacting self-stabilized network of asphaltene aggregates which added rigidity to the overall structure but resulted in an unstable colloidal structure because of the lower number of stabilizing resins[19]. Gel bitumens were observed to have low temperature susceptibility, low ductility, and a high aging rate [20,21]. Most bitumens were shown to exhibit properties characteristic of both bitumen types, suggesting that there exists sol or gel morphologies that are highly influenced by the SARA composition of a bitumen sample. Researchers therefore agreed that bitumen had molecular arrangements that spanned over multiple size domains and understanding the stability and energy distribu-

tion of the molecules in bitumen was key in effectively modelling its large-scale behavior.

Until this day, however, multiple interpretations and disputes exist on the size domain, shape, and stability of the molecular arrangements (and morphologies) of bitumen. Moreover, there are also disputes in what is the driving force behind the formation of these features (e.g., difference in molecular weights, polarities, etc.) and whether bitumen can be formally considered colloidal in nature. The presence of distinct molecular arrangements though, is undisputed, but a fully validated experimental interpretation of their nature remains to be published[3]. Recent work has used the thermodynamic principles that drive phase separation to provide a more thorough theoretical framework to explain the formation of different morphologies. They use special observation techniques to measure the stability, segregation rates, and equilibrium concentrations of a bitumen sample, and fit them to known phase separation models to validate their findings. These techniques are especially attractive because they provide a strong link between the chemical nature of a bitumen sample and its mechanical and rheological response. Moreover, they can aid in explaining the nature of the morphologies in bitumen, regardless of if they are colloidal or not. They are also helpful because many principles that have already been thoroughly tested in other complex mixtures can be applied to study bituminous materials.

2.2. Computational

The use of atomistic simulations, although challenging, have become pivotal in aiding scientists and engineers in developing a fundamental model of bitumen whose chemical characteristics can be linked to its mechanical and rheological response. Early use of QM and MD methods focused on obtaining the atomic structures of the molecules in bitumen, where scientists proposed multiple artificial atomic structures that fitted different experimental observations in terms of composition, functional groups, and solubility [22]. This allowed them to build larger simulations comprised of several molecules belonging to different SARA fractions and to study more complex intermolecular interactions. Even if the simulations involved the study of just a few molecules, researchers were already interested in exploring if the molecules would aggregate or cluster to form distinctive molecular arrangements. This was done mainly to show that the proposed atomistic models behave similarly to what had been observed experimentally. Many research articles found that asphaltene molecules aggregated into clusters, and most concluded that this clustering behavior resulted in energetically favorable conformations [23,24]. Researchers also demonstrated that the shape of the asphaltene molecules influenced the nature of the aggregation and showed that these aggregates could grow, break, and rearrange over nanosecond times [22,25–27]. Scientists also focused on answering how the presence of additional SARA fractions could result in energetically more favorable conformations. They demonstrated how the potential energy of these asphaltene clusters was substantially lower when surrounded by resinic molecules, strengthening the argument that bitumen had to have a molecular arrangement that favored the grouping of SARA fractions into features that resulted in lower and more uniform potential energy distributions [28–30].

Scientists then focused on creating a standardized set of molecules that could be used to build larger scale models of bitumen with molecules from all the SARA fractions present. These models still accounted for the elemental ratios and functional groups of a bitumen sample, but also differentiated between the SARA fractions on a molecular level. Numerous sets of molecules were proposed, each having notably different atomic structures, complexity levels, and molecule numbers[31,32]. Greenfield et. Al. [6,33] did a recollection of the different models available at the time and came up with a set of 12 molecules (2 for saturates, 2 for aromatics, 5 for resins, and 3 for asphaltenes) and different molecule numbers (for a total of 72) so that the number of molecules in each SARA category matched the elemental ratios and spectral analysis of different bitumen samples. Greenfield's molecular set has been widely adopted as a basis to build bituminous materials in MD simulations as the models that can be built result in accurate and stable physical properties, account for different SARA components in bitumen, and are highly customizable. Several research articles have been published using Greenfield's molecular set [34–38], often including slight atomic modifications to fit the models to a specific bitumen sample, or to mimic certain conditions like those of bitumen aging.

Most of the research articles involving bitumen derived from Greenfield's model focus on measuring larger scale thermodynamic, mechanical, or rheological properties. This is mainly because researchers are ultimately interested in linking the aspects of a fundamentally described chemical system with properties that are more relevant to the fields of Civil and Pavement Engineering. However, few of these articles emphasize on the clustering behavior that these molecules exhibit over the course of the simulations performed. These models are built by homogeneously distributing all the molecules in a simulation box, creating a bitumen model whose molecules are uniformly dispersed regardless of their SARA fraction, and whose molecular arrangements are not accounted for in the simulations. Measurement of their properties is done as soon as the models attain numerical equilibrium of some of its most fundamental thermodynamic quantities, ignoring that these atomistic models of bitumen may exhibit phase behavior and rearrange to form well-defined intermolecular arrangements. Greenfield acknowledged this and argued that the size and time domain needed for some of these features to manifest is significantly larger and longer than the ones used in the MD model proposed and that the results obtained were accurate enough for their line of research [5,6]. However, subsequent simulations performed by several scientists involving larger and more complex models continued to use an initially homogeneous distribution of molecules, raising the question on whether a bitumen model built using this method is prone to exhibit significant phase behavior if the model is enlarged and run over exceedingly long simulation times.

Researchers acknowledge that exploring a larger size and time domain would be beneficial to realistically model bituminous materials [39–43]. This is because the largest models proposed until now do not surpass a few hundred molecules in size and the longest simulations involve a few nanoseconds in simulation time. Researchers also acknowledge that exploring a larger size and time domain would have to involve the study of phase behavior phenomena, where molecules of similar SARA fractions are expected to cluster and form distinctive molecular arrangements [44,45]. Scientists have used Coarse Grained methods to effectively reproduce the behavior of bitumen molecules using beads that approximate a few atoms into a single particle. This has allowed them to increase the size and time domain explored by an order of magnitude with a certain loss of accuracy in their molecular models. Most of the articles published seek validation of their proposed models by showing how the molecules exhibit phase behavior, and how different SARA fractions rearrange, aggregate, stack, or lump over considerably long simulations times[43–47]. They also state that having the ability to explore the rearrangement of molecules allows them to study the impact that a possible colloidal structure would have in the thermodynamic and rheological properties of bitumen[43–46]. However, the parameters and expressions used to perform these simulations vary significantly between articles, indicating that their use, although promising, still require further work.

Even though researchers successfully showcase how their bitumen simulations exhibit phase behavior, until now, they have not explicitly studied how far into the simulations can the models exhibit phase behavior; they often report it as an expected consequence that stems from the nature of the intermolecular interactions present in their model. However, none have use special techniques to quantify and track how each SARA fraction rearranges over time. Moreover, none have studied if there exists a molecular arrangement that result in a bitumen model that is much closer to its equilibrium form, effectively shortening the time (and energy) required to prepare a truly stable model of bitumen. Having the ability to manually place molecules of different SARA fractions into different arrangements would allow scientists to build bitumen models with a specific phase separation degree in a much shorter time. It could also lead to the formation and control of well-established morphologies in numerical models found in gel and sol bitumens, whose shape, size, and stability are known to have considerable influence over the mechanical and rheological properties of bitumen. Any development done to explore the extent and the impact of phase separation could potentially benefit both conventional MD simulations and Coarse-Grained methods, as well as larger scale continuum methods in need of a specific geometric arrangement of the molecules in bitumen.

3. Simulation basis

This stage consists of determining the initial basis of assumptions that remain constant in all the MD simulations performed. These include determining the molecular set and numbers used to represent bitumen (and its SARA components) in a computational environment, selecting the force field expressions, types, and charges used to describe the atomic interactions, establishing the numerical parameters (e.g., integration method, time step), defining the simulation types and conditions, and determining which set of tools are going to be used to perform the simulations effectively and efficiently. The simulations of this study were performed on the DelftBlue High Performance Computing Centre (DHPC)[48].

3.1. Molecular set

The molecular set used in this study is from Shisong et Al., which is essentially Greenfield's original set but with different molecule numbers and small molecular modifications to match the SARA fractions and functional analysis to those on a bitumen sample from TotalEnergies (PEN Grade 70/100). The total number of molecules in the bitumen models of this study is eight times larger than the one used by Shisong et al., for a total of 608 molecules per model consisting of 24 saturates, 328 aromatics, 208 resins, and 48 asphaltenes, with an overall atomic formula of $C_{19528}H_{26272}O_{176}N_{64}S_{248}$, an average molecular mass of 448.51 g/mol, and an estimated average density of 1.010 g/cm^3 at 298 K and 1 atm. The size of the model is selected to be substantially larger to allow for a clearer formation of molecular arrangements of a size that is within the domain of colloidal dispersions (of at least 15 Å in diameter)[49] while still keeping the simulation times within reasonable limits. Moreover, the models of bitumen that are larger have a lower potential energy (~1400 kJ/kg against ~ 1700 kJ/kg), which could be attributed to diminished effects of periodic boundary conditions and to the smaller relative size of the molecules when compared to the size of the whole model. The list of molecules and SARA fractions used to build the bitumen models of this study are presented in Table 1. The chemical structure of the molecules used is presented in Fig. 2.

The molecules in the bitumen models of this study are labelled depending on the SARA fraction they belong to. The atoms belonging to the *Asphaltenes* or the *Resins* are treated as separate groups and are labelled with an *A* and *R*, respectively. The saturates and the aromatics are grouped into a single, homogeneously mixed phase, labeled with an *Sa*. The saturates and the aromatics are grouped together because they are known to coexist in the same phase and the number of saturate molecules in the MD model is too small to exhibit distinctive phase behavior on its own (e.g., crystallization).

3.2. 3.2. Numerical integrator

MD simulations predict the properties of chemical models by calculating the positions, velocities, and accelerations of particles, or atoms, by using an integrator to solve the Newtonian equations of motion under the influence of specified force fields[50,51]. The relation between the acting forces and an atom's position is given by[52]

$$F_i = \frac{\partial^2 n_i}{\partial t^2} \cdot m_i \tag{1}$$

where F_i is the resulting force acting on atom i, n is the position coordinate (e.g., x, y, or z), and m_i is the particle's mass. The Velocity Verlet integrator method is used throughout this study as it is widely used in MD simulations, and because it is accurate, efficient, and avoids energy drifts after considerably long simulation times [53]. The numerical integrator obtains atomic trajectories by iteratively computing the particles' forces at discrete time steps (δt). The time step must be small enough to maintain numerical stability and accuracy, but large enough to save computational time and resources. The time of the integration step used throughout this study is estimated by using

$$\delta t = \frac{f}{10} = 1\,\text{fs} \tag{2}$$

where f is the time frequency required to describe the fastest vibration term of the force field in a model composed of bitumen molecules from Table 1, which corresponds to the C–H and O–H bond vibration frequencies of approximately $f = 11fs$ (3100 cm^{-1})[54]. Other research papers involving bituminous models also use a δt equal to 1 fs.

3.3. Force field

Force fields are used by the numerical solver to compute the forces acting on the atoms of a model on each integration step. They can be interchangeably expressed as potential energy functions since the relation between the force acting on the model of atoms and their energy is given by

$$\boldsymbol{F} = -\nabla \boldsymbol{E} \tag{3}$$

where $\boldsymbol{F}$ is the force field, and $\boldsymbol{E}$ is the potential energy function. Force fields often contain multiple terms that account for the force contribution of different types of interactions (e.g., Van der Waals, electrostatic forces, etc.). The total potential energy in a model of atoms governed by a force field is given by

$$\boldsymbol{E} = \sum \boldsymbol{E}^x \tag{4}$$

where x represents each of the terms. An atomic model is said to be at equilibrium if the acting forces on all its atoms is close to zero, resulting in stable, lower energy conformations that should resemble those found in experimental observations[55]. Several force fields (and their respective input parameters) that cover complex organic mixtures have been published and choosing one which real-

Table 1
List of molecules and SARA fractions used in the bitumen models of this study.

SARA Fraction		Name	Chemical formula	Mass (g/mol)	Density (g/cm^3)	Amount in model	Mass ratio (%) Model	Mass ratio (%) Experiment
Sa	Saturates	Squalane	$C_{30}H_{62}$	422.8	0.803	16	2.48	3.90
		Hopane	$C_{35}H_{62}$	482.9	0.913	8	1.42	
	Aromatics	Dioctyl-cyclohexane naphthalene (DOCHN)	$C_{30}H_{46}$	406.7	0.916	168	25.1	53.3
		Perhydrophenanthrene naphthalene (PHPN)	$C_{35}H_{44}$	464.7	1.030	160	27.8	
R	Resins	Quinolinohopane	$C_{40}H_{59}N$	553.9	1.007	24	4.88	30.3
		Thioisorenieratane	$C_{40}H_{60}OS$	589.0	1.010	24	5.18	
		Benzobisbenzothiophene	$C_{18}H_{10}OS_2$	306.4	1.540	104	11.7	
		Pyridinohopane	$C_{36}H_{57}N$	503.9	0.977	24	4.43	
		Trimethylbenzeneoxane	$C_{29}H_{50}O$	414.7	0.893	32	4.87	
A	Asphaltenes	*Phenolic** asphaltene	$C_{42}H_{54}O$	574.9	1.049	16	3.37	12.8
		*Pyrrolic** asphaltene	$C_{66}H_{81}N$	888.4	1.104	16	5.21	
		*Thiophenic** asphaltene	$C_{51}H_{62}S$	707.1	1.100	16	4.15	

***Note:** The names *phenolic*, *pyrrolic*, and *thiophenic* refer to the characteristic functional group present on each asphaltene molecule, and not to the name of the *chemical compound* itself. The overall structure of the asphaltenes is artificially obtained by matching them to observations, and do not correspond to molecules known to realistically exist.

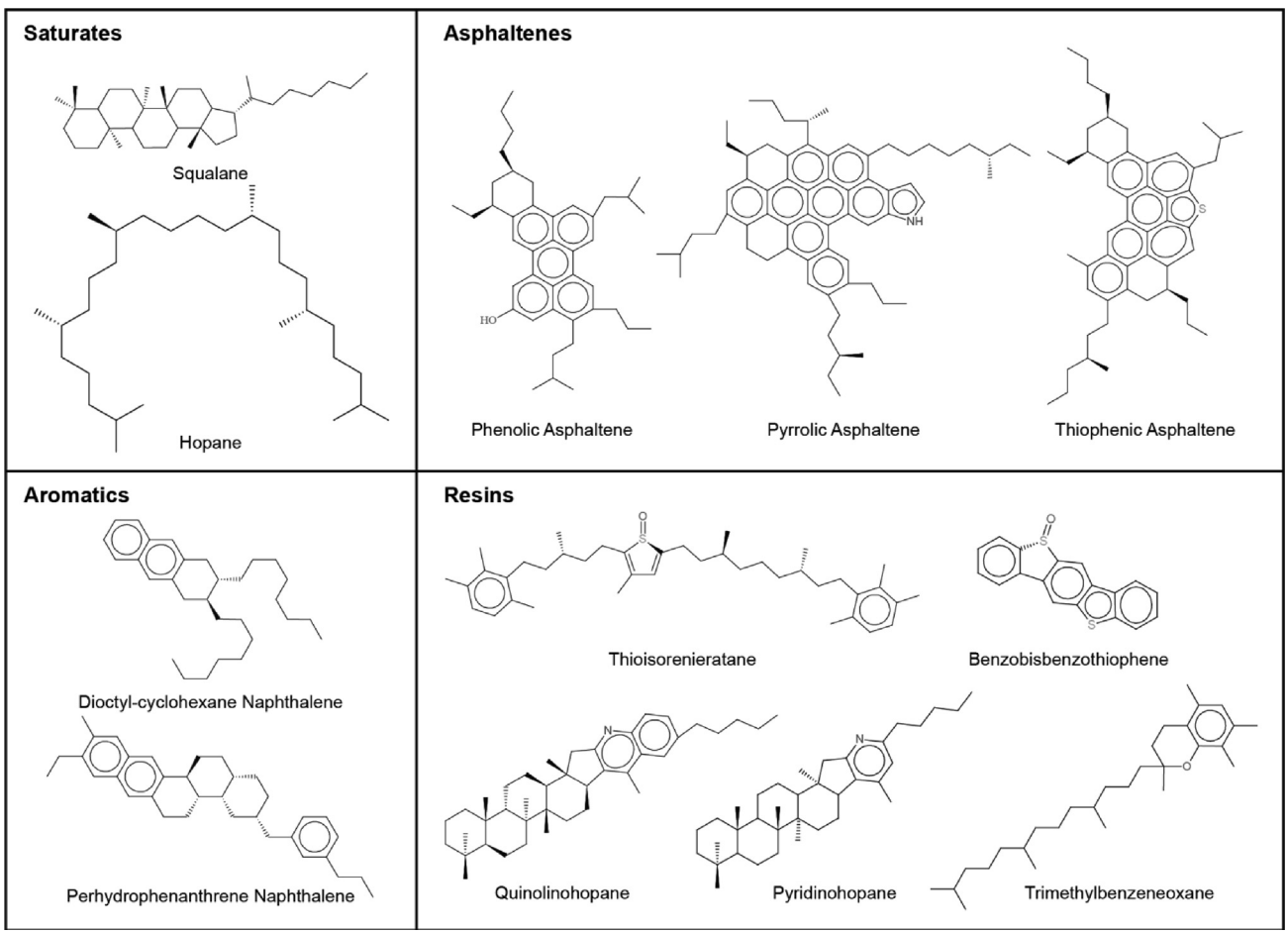

Fig. 2. Chemical structure of the molecules used in this study. The symbols O, N, and S represent Oxygen, Nitrogen, and Sulfur respectively. The bold and dashed lines denote the stereochemistry of the molecules.

istically predicts the properties of a model of bitumen is important to accurately mimic its real-life behavior. These force fields should be able to model C, H, O, N, and S interactions and account for electron delocalization, polarity, and resonance effects, which are known to play an important role in the molecular stacking of certain molecules and molecular arrangements in bitumen.

Three different force fields are tested to determine their capacity to measure the density, specific heat capacity (at constant volume), and thermal expansion coefficient of three bitumen models accurately and efficiently at 298 K and 1 atm. These are the Polymer Consistent Force Field (PCFF), the Consistent Valence Force Field (CVFF), and the COMPASS[56] force field. The results of Table 2 indicate that the three force fields are able to realistically predict the density, heat capacity, and thermal expansion coefficient of bitumen when compared to experimental results. However, the PCFF is substantially faster than the other two. This

Table 2
All the force fields (the PCFF, the CVFF, and the COMPASS) produced accurate results, but the PCFF was substantially faster and is therefore used in the MD simulations of this study.

Property (298 K, 1 atm.)	Model	PCFF	CVFF	COMPASS	Liter.
Density	1	1.031	1.031	1.031	1.010
[g/cm^3]	2	1.032	1.032	1.032	
	3	1.031	1.031	1.031	
Specific Heat Capacity	1	2.11	2.13	2.10	2.05
[kJ/kg/K]	2	2.09	2.15	2.10	
	3	2.09	2.16	2.11	
Thermal Expansion [1/K]	1	1.53	1.48	1.55	1.50
($\cdot 10^4$)	2	1.49	1.54	1.59	
	3	1.50	1.55	1.57	
Time to complete (normalized to PCFF)	1	1.00	1.12	1.17	–
	2	1.00	1.12	1.18	
	3	1.00	1.13	1.17	

could be because the PCFF handles certain situations that are ubiquitous in bitumen models (e.g., electron delocalization due to the stacking of aromatic rings) by means of using a previously computed table of values instead of computing them on demand. Moreover, instantaneous model properties (e.g., potential energy, temperature, or density) stabilized faster with the PCFF, reducing the computational time needed to complete simulations. As a result, the simulations run later in this study are performed using the PCFF.

The total potential energy in a model governed by the PCFF is given by the sum of 12 different interaction terms,

$$E_{PCFF,total} = \sum E^b + E^{ia} + E^{oa} + E^t + E^{bb} + E^{ba} + E^{bt} + E^{aa} + E^{at} + E^{tt} + E^{VDW} + E^{coul} \quad (5)$$

where each energy term E^x is described in Table 3.

To save computational time, short-range Van der Waal interactions (E^{VDW}) with particles separated by a distance beyond $r_c = 2.8r_{ij}^0$ are neglected using the cut-and-shift method as their interatomic energy becomes smaller than 0.1% of the energy that would exist if the atoms were at equilibrium positions[57]. Therefore, the potential energy term E^{VDW} becomes:

$$E^{VdW}(r_{ij}) = \begin{cases} E(r_{ij}) - E(r_c)\, if r_{ij} < 2.8r_{ij}^0 \\ 0\, if r_{ij} \geq 2.8r_{ij}^0 \end{cases} \quad (6)$$

where r_{ij}^0 is the non-bonded interatomic distance of E^{VdW}. Long-range Coulomb and Van der Waals interactions are handled with the PPPM[58] method and by applying tail corrections[59] respectively.

Table 3
List of potential energy terms in the PCFF. The symbols i, j, k, l, and m refer to the group of atoms involved in the calculation, r_{ij} is the interatomic distance, θ_{ijk} and χ_{ijk} are the in-plane and out-of-plane angles formed by three consecutively bonded atoms, φ_{ijkl} is the dihedral angle formed by four consecutively bonded atoms, M is the multiplicity of the potential at which E^x becomes zero, k, r^0, θ^0, χ^0, φ^0, s_0, ϵ_{ij} and ε_0 are force field constants that depend on the nature of the atomic group involved in the calculation, and q_i is the partial atomic charge.

Description	Expression
Bond bending	$E^b = \sum_{ij} \sum_{M=2}^{4} k_{(m)ij} \left(r_{ij} - r_{ij}^0\right)^m$
In-plane angle bending	$E^{ia} = \sum_{ijk} \sum_{M=2}^{4} k_{a,ijk}^m \left(\theta_{ijk} - \theta_{(m),ijk}^0\right)^m$
Out-of-plane angle bending	$E^{oa} = \sum_{ijk} k_{ijk} \cdot \left(\chi_{ijk} - \chi_{ijk}^0\right)^2$
Symmetric torsional angle bending	$E^t = \sum_{ijkl} \sum_{m=1}^{4} k_{(m)\,ijkl} \left(1 + \cos\left(m\varphi_{ijkl} - \varphi_{(m)ijkl}^0\right)\right)$
Cross-coupling bond-bond	$E^{bb} = \sum_{ijkl} k_{ijkl} (s_{ij} - s_{0,\,ij})(s_{kl} - s_{0,\,kl})$
Cross-coupling bond-angle	$E^{ba} = \sum_{ijk} k_{ijk} (r_{ij} - r_{0,\,ij})(\theta_{ijk} - \theta_{0,\,ijk})$
Cross-coupling bond-torsion	$E^{bt} = \sum_{ijkl} \left(r_{ij} - r_{ij}^0\right) \sum_{m=1}^{3} k_{(m)\,ijkl} \cos\left(m\varphi_{(m),ijkl}\right)$
Cross-coupling angle-angle	$E^{aa} = \sum_{\substack{angle ijk,\\ angle jkl}} k(\theta_{ijk} - \theta_{0,ijk})(\theta_{jkl} - \theta_{0,jkl})$
Cross-coupling angle-torsion	$E^{at} = \sum_{ijkl} \left(\theta_{ijk} - \theta_{ijk}^0\right) \sum_{m=1}^{3} k_{(m)ijkl} \cos(m\varphi_{(m),ijkl})$
Cross-coupling torsion-torsion	$E^{tt} = \sum_{ijklm} k_{ijklm} \cos(\varphi_{ijkl}) \cos(\varphi_{jklm})$
Van der Waals repulsive / attractive	$E^{VdW} = \sum_i^N \sum_{i \neq j}^N \epsilon_{ij} \left[2\left(\frac{r_{ij}^0}{r_{ij}}\right)^9 - 3\left(\frac{r_{ij}^0}{r_{ij}}\right)^6\right]$
Electrostatic (Coulomb)	$E^{coul} = \frac{1}{4\pi\varepsilon_0} \sum_i^N \sum_{i \neq j}^N \frac{q_i q_j}{r_{ij}}$

4. Simulation schemes

In this study, there are nine MD simulation schemes used to initialize, control, and achieve a desired molecular arrangement or thermodynamic state:

4.1. Insertion

This step consists of using a Python/PyPy script to insert molecules into the simulation box by using a quasi-random Sobol distribution method so that the molecules are distributed more evenly and overlap the least possible. The Sobol distribution is specifically designed to generate an even distribution of points in three dimensions likely to produce a lower energy distribution of points when compared to less discretized methods at no additional computational cost. The molecules are not allowed to occupy positions near other atoms already present in the simulation box (a distance $r_{ij}^0/2$ or less) to prevent exceedingly high potential energies that arise from atoms being too close to each other. If needed, the molecules can be placed away from the walls so that that they are confined within the boundaries of the simulation box. The molecules' bonds and angles are kept rigid when placing and distributing them throughout the simulation box; the molecules are translated and rotated as a rigid group of atoms preserving their original spatial conformation. The atomic positions for each of the molecules inserted are initialized by using their corresponding SMILES notation, followed by a simple energy minimization step that produces a relatively stable conformer of the molecules in three dimensions.

4.2. Minimization or optimization

This technique consists of manually changing the positions of the atoms so that the forces between the molecules reach an equilibrium (i.e., a local minimum on the potential energy surface of the model). This scheme is performed using the Large-scale Atomic/Molecular Massively Parallel Simulator (LAMMPS) using a

conjugate gradients method, until there is no further decrease in potential energy and the total forces of the model have converged to within two decimal places.

4.3. NPT

MD run where the pressure and temperature are controlled by a modified Nose-Hoover thermostat that incorporates a drag factor to reduce oscillatory effects, with a pressure and temperature damping factors equal to 100 fs, and a particle velocity drag coefficient equal to 1.0.

4.4. NVT

MD run where the temperature is controlled by a modified Nose-Hoover thermostat that incorporates a drag factor to reduce oscillatory effects, with a temperature damping factor equal to 100 fs, and a drag coefficient equal to 1.0.

4.5. NVE

MD run where no energetic control is used. The particles' motion is dictated entirely by the interactions computed by the force field.

4.6. Equilibration

An equilibration stage is a period of time required for the atoms to reach lower energy positions in response to a variation in the model conditions, where the total forces and the potential energy of the model need to remain constant after a certain time. It is done using *NPT* or *NVT* dynamics and is taken to be as twice the time required to stabilize the model's forces and energy to within 0.5% of their new average value. The input parameters for the *NPT* or *NVT* stages remain unchanged unless explicitly specified.

4.7. Compression

A compression stage in this study consists of manually resizing the boundaries of the simulation box to a desired value and repositioning all the atoms in the model in proportion to the applied volumetric change. The compression rate involves applying a true strain rate given by

$$\varepsilon_{\text{true}} = \frac{\log\left(\frac{z_f}{z_0}\right)}{t}, \tag{7}$$

where z_0 and z_f are the initial and final dimensions of the simulation box in the z direction, and t is the total simulation time of the compression scheme.

4.8. Stability run

The objective of this scheme is to find out whether the molecular arrangement of the *Sa*, *R*, and *A* fractions within a bitumen model would rearrange or mix over a considerably long time at 298 K and 1 atm. The bitumen models are subjected to *NPT*, *NVT*, and *NVE* runs performed in series to evaluate the stability of the bitumen models (and its properties) when exposed to environments with decreasing levels of energy control. The use of *NVE* dynamics is crucial to determine whether the model is not artificially kept stable by the energy controls implemented in the integrator algorithms. The length of each of the simulation stage is set to be 50 ns long. The overall time elapsed in a *stability run* (150 ns) is considered to be a significantly long simulation time in MD simulations of this kind. It is selected to be ten times the average time needed for a bitumen molecule to diffuse away a distance equal to its average diameter, given by:

$$\tau = 10\frac{d_A^2}{D_{self}^{lit}}, \tag{8}$$

where d_A is taken to be equal to 8.66 Å, and D_{self}^{lit} is the average self-diffusion coefficient of a molecule in a bitumen model at 298 K, equal to 1e-11 m^2/s (see Section 7.8, *Self-diffusion Coefficient*). The integration step is kept at δt equal to 1 fs.

4.9. Heating cycle

The aim of this test is to study the effect that a high temperature cycle has on the morphology of the bitumen models of this study, and to evaluate whether higher temperatures would favor increased phase behavior. The *heating cycle* is performed at a constant pressure of 1 atm. and at a maximum temperature of 433 K, which represent typical conditions when preparing *Hot Mixed Asphalt* in which bitumen is exposed to the highest temperature of its service life[60]. The *heating cycle* is performed in five stages:

(1) Constant temperature at 298 K (3 ns).
(2) Heating up to 433 K (2 ns).
(3) Constant temperature at 433 K (10 ns).
(4) Cooling down to 298 K (2 ns).
(5) Constant temperature at 298 K (3 ns).

The first step consists of running *Equilibration* dynamics using *NVT* and *NPT* schemes (in that order), each 1 ns and 2 ns long respectively to reinitialize the simulation environment and seamlessly reintroduce energy control schemes into the simulation. The second step consists of running an *NPT* stage 2 ns long, where the models are heated from 298 K to 433 K at a rate of 0.10 K/ps. A slower heating rate is achieved by modifying the pressure and temperature damping factors of the *NPT* scheme to 1000 fs and changing the particle velocity drag coefficient to 1.85 to extend the time needed for the temperature to rise to 433 K. In the third step, the temperature is maintained for 10 ns using *NPT* dynamics to test the stability of the molecular arrangements in a high temperature environment for a relatively long time. The fourth step consists of cooling the model back to 298 K for 2 ns using *NPT* dynamics with the Nose-Hoover factors of the second stage. The fifth step involves running a series of MD simulations with decreasing levels of energy control to evaluate the state of the model at the end of the *heating cycle*. This stage consists of *NPT*, *NVT*, and *NVE* stages run in series, each 1 ns long.

5. Model construction methods

This section consists of initializing, controlling, and running a series of MD simulations to successfully obtain stable models of bitumen with a particular molecular arrangement of its *Sa*, *R*, and *A* fractions. The final dimensions of the simulation boxes in the bitumen models of this study are approximately equal to 50, 50, and 200 Å for the x, y, and z axes respectively so that their final density is roughly equal to 1.010 g/cm^3. The length of the box's side in the *z* dimension is purposedly selected to be four times the length of the *x* and the *y* dimensions so that there is enough space for multiple arrangements to form across one dimension while saving computational resources given that the size of the models has already been chosen to be eight times larger than those built by Greenfield. The length of *z* as a function of the model's density (ρ) is given by

$$z(\rho) = \frac{N_m \cdot M}{x \cdot y \cdot \rho \cdot N_{av}} \tag{9}$$

where N_m is the number of molecules, M is the average molecular mass, x and y are both equal to 48 Å, and N_{av} is Avogadro's number. The values of x and y are kept constant throughout the simulation as the models are compressed only by shortening the length of z. Two different methods (the *Conventional Method* and the *Heterogeneous Method*) are attempted to build the bitumen models and are thoroughly described as follows.

5.1. Conventional method

The *Conventional Method* replicates the construction method used by the majority of the researchers currently working on computational models of bitumen, consisting of a total of five steps performed in series. The first step in this method consists of homogeneously placing individual molecules in a low-density box of dimensions x,y, and z equal to 48, 48, 1000 Å respectively by applying an *Insertion* step (see *Simulation Schemes*). A low density is necessary to decrease the likelihood of having overlapping atoms between the molecules inserted. The values of x,y, and z are obtained using Equation (8) for an initially low density of $\sim$ 0.20 g/cm^3. The molecules are placed at a distance of 25 Å away from the walls in the z-direction so that that molecules are confined within the boundaries and the model can be uniaxially compressed to its equilibrium density in later stages. Multiple low-density models are generated until there are enough desired where the maximum potential energy of the atoms is equal or less than 150 kJ/mol/atom. The latter is simply selected to be 20 times the average potential energy of the atoms in an equilibrated bitumen model, so that the initial positions of the atoms in the newly created models can be equilibrated without exceedingly rigorous control techniques. The second step consists of loading the models into LAMMPS, assigning the atoms' force field types and charges, and optimizing the atomic positions so that they accommodate more natural energetic configurations in response to the more accurate (but computationally more expensive) force field dynamics. The latter is achieved by running a *Minimization* stage (see *Simulation Schemes)* until the models' molecules reach stable conformations and the forces and the energy of the models stabilize. In the third step, the resulting low-density models are compressed to the natural target density of bitumen of $\sim$ 1.010 g/cm^3 in a series of *Compression* and *Equilibration* stages. The *Compression* stages are performed uniaxially in the z direction, keeping the x and y dimensions constant, while applying decreasingly small compressions every 5000 integration steps (i.e., using a true engineering strain given by Equation (7)). The *Equilibration* stages consist of running *NVT* dynamics 50 ps long to allow the molecules to occupy lower energy conformations in response to the strain added by the variation in the model's geometry. The fourth step consists of removing the walls in the z direction previously used to compress the models to subject the models to full periodic boundary conditions with an *Equilibration* using an *NPT* dynamics stage 10 ns long. The fifth step consists of subjecting the models to two consecutive *Equilibration* stages using *NVT* and *NVE* dynamics 10 ns each so that the molecules occupy consistent energy arrangements, and the model's properties remain constant over time without the need of a barostat or a thermostat. A schematic representation of the steps followed in the *Conventional Method* is presented in Fig. 3.

5.2. Heterogeneous method

This method consists of inserting the molecules corresponding to each *Sa*, *R*, and *A* fraction in Table 1 at separate times during a simulation so that each group of molecules has time to occupy more natural positions and form more realistic molecular arrangements (e.g., clusters, lumps, or shells) on their own. This is achieved by first inserting the molecules of a particular *Sa*, *R*, or *A* fraction in a low-density simulation box, running an *NVT* dynamics step, repeating the process until all the SARA fractions are inserted, and compressing the model until its pressure is 1 atm. (with target density of $\sim$ 1.010 g/cm^3). The resulting model is then subjected to a series of *Equilibration* steps where its thermodynamic properties reach an equilibrium and remain stable over time. The *A* molecules are added first, the *R* molecules second, and the *Sa* molecules third. This insertion order reproduces the layering order of the proposed colloidal nanostructure of bitumen, where asphaltenes cores surrounded by resinic shells form colloidal particles which are dispersed in a medium of saturates and aromatics.

The *Heterogeneous Method* consists of twelve steps which are run in series. The first step involves inserting only the molecules corresponding to the *A* fraction into a low-density box of dimensions x,y, z equal to 48, 48, 1000 Å respectively by using an *Insertion* step (see *Simulation Schemes*). The second step consists of loading the models into LAMMPS and running a *Minimization* stage (see *Simulation Schemes)* until the models' molecules reach stable conformations and the forces and the energy of the models stabilize. The details of steps 1 and 2 are similar to those of step 1 and 2 of the *Conventional Method*. The third step consists of running an *NVT* dynamics stage 1 ns long, to allow the molecules to form more natural molecular arrangements (e.g., clusters, lumps, or shells). Different frames (or copies of the model) are extracted at various times throughout this step so that the heterogeneity of subsequent models can be established by the structure of the clusters at that point in time. Highly *homogeneous* models are created by extracting the positions of molecules at the beginning of the *NVT* simulation, where there are no (or few) clusters formed yet, to produce more uniformly mixed models. *Heterogeneous* models are generated by extracting the position of molecules at later points in time during the *NVT* simulation, so that there are larger and fewer asphaltene clusters, resulting in an increasingly differentiated distribution of the *Sa*, *R*, and *A* fractions. The fourth step consists of placing the molecules corresponding *R* fraction into the models extracted in step 3 by using an *Insertion* step. In the fifth step, the models are loaded back into LAMMPS like in step 2. The sixth step consists of running an *NVT* dynamics stage 10 ns long, where the molecules from the *A* and *R* fractions are allowed to interact and produce more natural molecular arrangements. In the seventh step, the molecules corresponding to *Sa* fraction are placed into the remaining empty space in the simulation box by applying an *Insertion* step. In the eighth step, the models are loaded back into LAMMPS like in the second and fifth step. In the ninth step, an *NVT* dynamics stage of 10 ns is run to allow the newly inserted SARA fraction to occupy more natural arrangements. In the tenth step, the resulting low-density models are compressed to the natural target density of bitumen of $\sim$ 1.010 g/cm^3 in a series of *Compression* and *Equilibration* stages just like in step 3 of the *Conventional Method*. The eleventh step consists of removing the walls in the z direction previously used to compress the models to subject them to full periodic boundary conditions with an *Equilibration* stage using *NPT* dynamics 10 ns long. The twelfth step consists of subjecting the models to two consecutive *Equilibration* stages using *NVT* and *NVE* dynamics 10 ns each so that the molecules occupy consistent energy arrangements, similarly to what is done in Step 5 of the *Conventional Method*. A schematic representation of steps in the *Heterogeneous Method* is presented in Fig. 4.

6. Measurement stage

The molecular models of bitumen built using the *Conventional Method* and the *Heterogeneous Method* are subjected to a series of

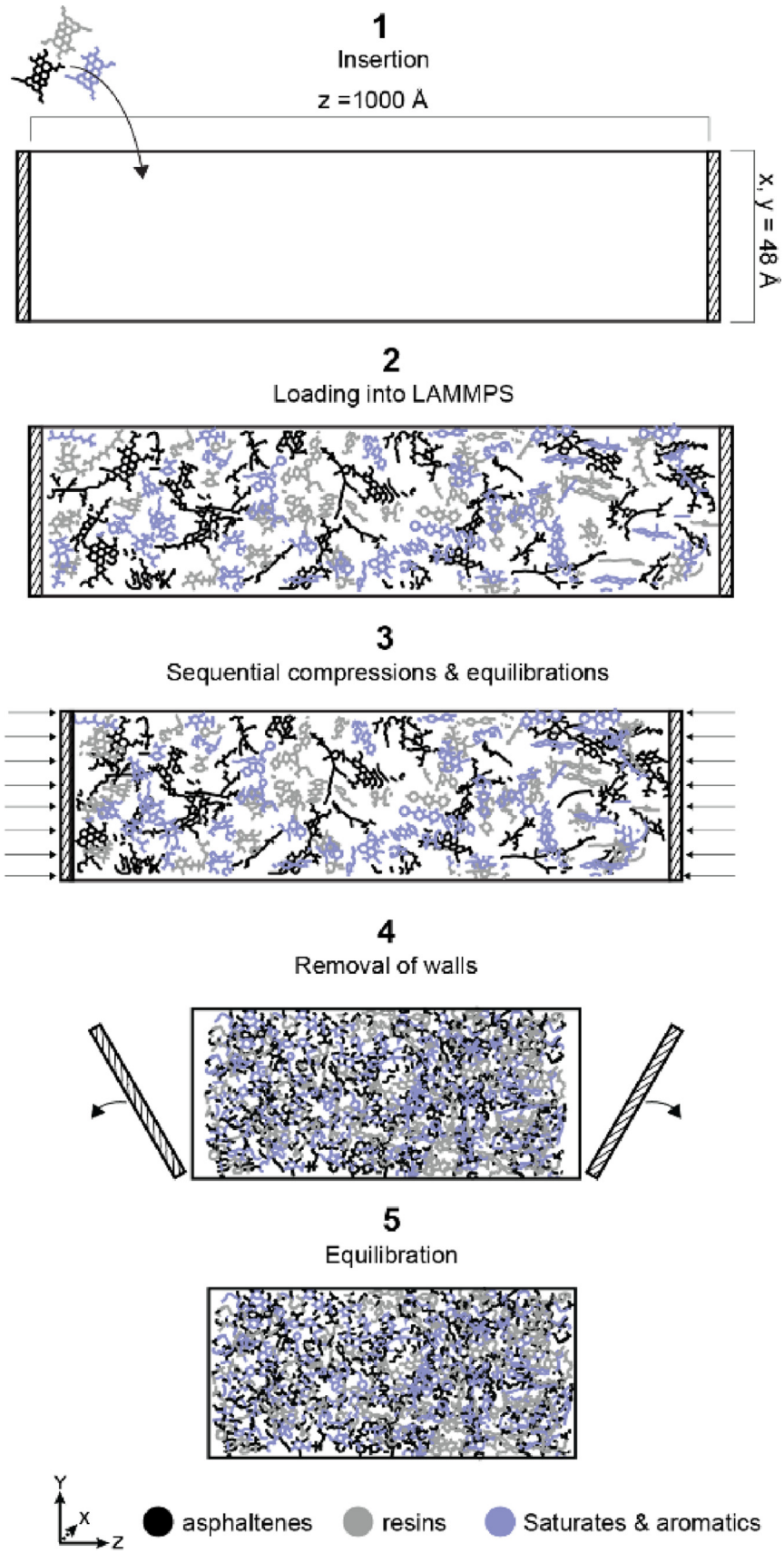

Fig. 3. In the *Conventional Method*, all the molecules from Table 1 are homogeneously distributed throughout the simulation box, resulting in a bitumen model whose molecules are equally dispersed regardless of the SARA fraction they belong to.

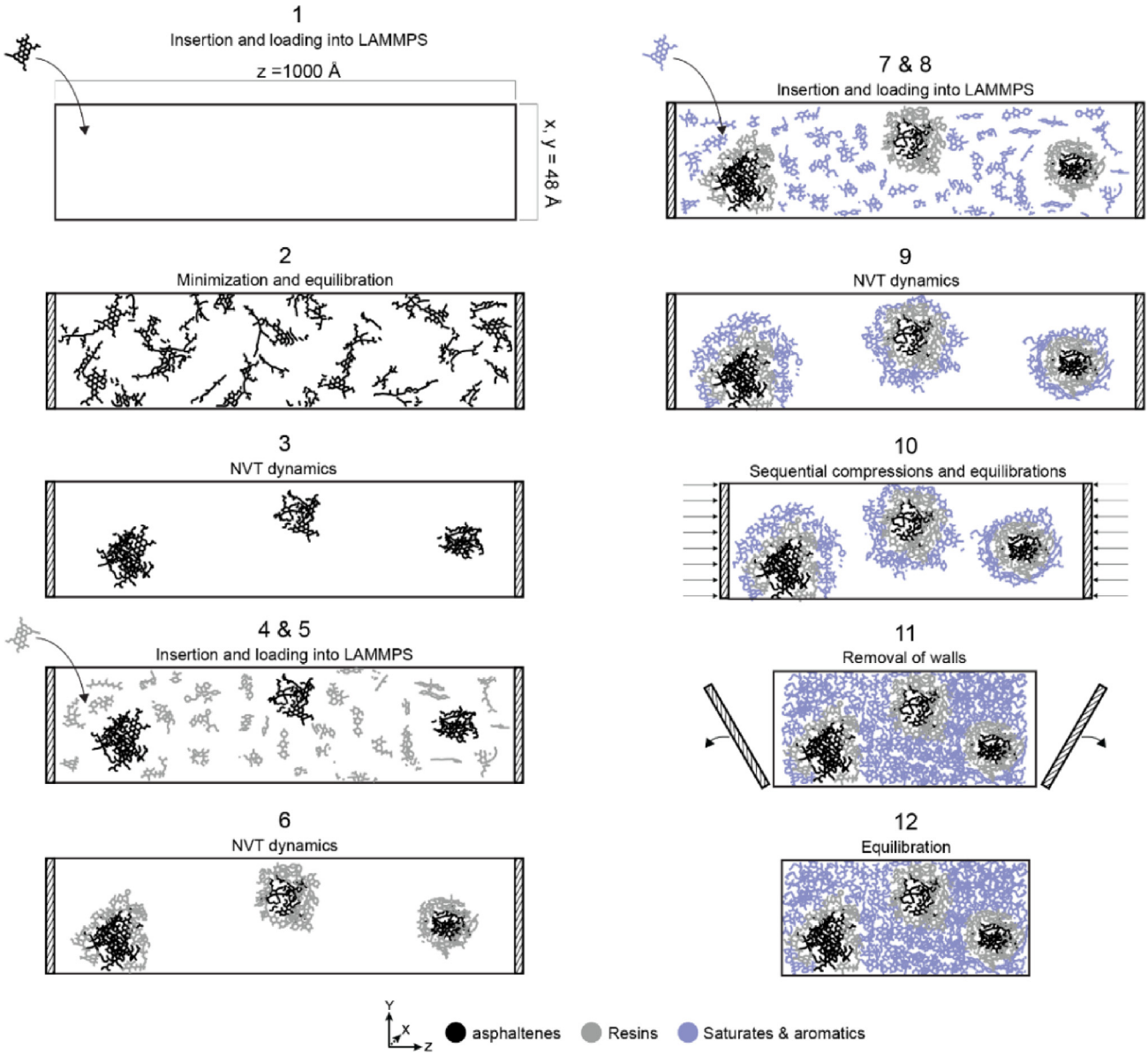

Fig. 4. In the *Heterogeneous Method*, the formation of core–shell structures inside the bitumen model is achieved by first distributing the molecules of the *A* fraction in a low-density simulation box, running an NVT dynamics stage to allow for molecular clusters to form, repeating the process until all the molecules from the *R*, and the *Sa* fractions are inserted, and compressing the model until its pressure and density are 1 atm. and $\sim$ 1.010 g/cm^3 respectively.

MD runs after they have been built to assess whether these models are computationally and thermodynamically stable and accurate, and to track the arrangement of the *Sa*, *R*, and *A* fractions to evaluate whether their molecular arrangements is stable and in equilibrium. These are first subjected to a *stability run*, followed by a *heating cycle*, followed again by another *stability run* (see *Simulation Schemes* for more details). The properties of the models are evaluated and compared in each of the following points in time throughout the simulations:

(1) At the end of the removal of the periodic boundary conditions (step 4 of the *Conventional Method* and step 11 of the *Heterogeneous Method*).
(2) At the end of the *NVE Equilibration* step (step 5 of the *Conventional Method* and step 12 of the *Heterogeneous Method*).
(3) At the end of the first *stability run*.
(4) Right after the model has been heated up to 433 K.
(5) At the end of the high temperature segment of the *heating cycle* (at 433 K).
(6) Right after the model has been cooled back down to 298 K.
(7) After the second *stability run* has finalized.

These numbered points are depicted in Fig. 5 and are used to rapidly refer to relevant points of interest to analyze the results of the MD simulations of this study.

7. Analysis

7.1. Neighboring atoms

Two atoms are considered to be *neighbors* if they are bonded or if the energy between them is larger than 0.1% of the equilibrium energy computed by the force field[51,55,61]. In other words, neighboring atoms are those that are within non-negligible

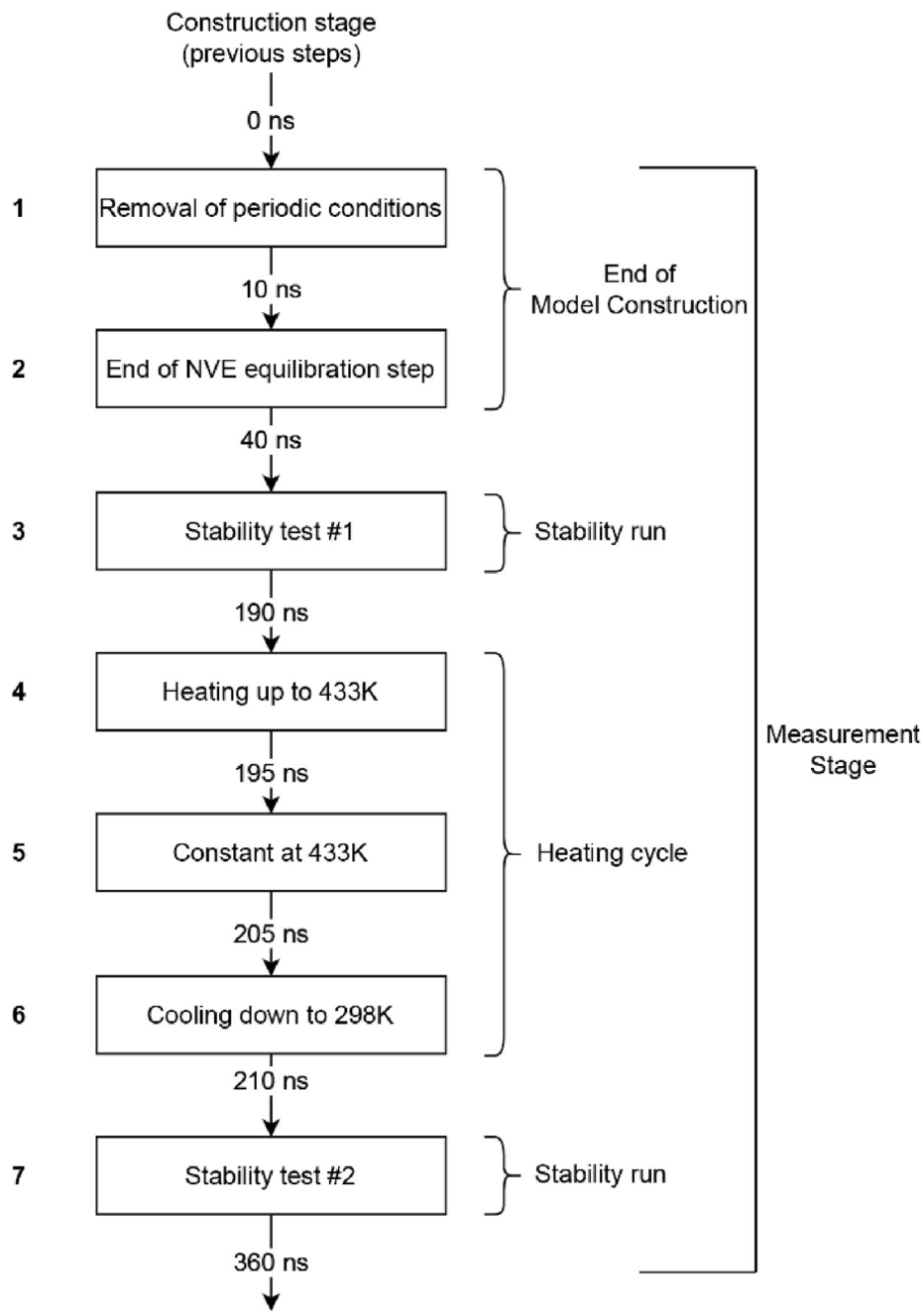

Fig. 5. The properties of the bitumen models are measured and compared in the *Results* section in each of the following points in time throughout the simulations.

interaction range given by the force field, equal to a distance equal or less than r_{ij}^{0}.

7.2. Neighboring fractions

The distribution of the *Sa*, *R*, and *A* fractions in the bitumen models is used to keep track of how the molecules corresponding to each fraction rearrange throughout the simulation, indicating if there is phase separation between the molecules. This is achieved by counting the number of *Sa*, *R*, and *A* atoms that neighbor each fraction *Sa*, *R*, and *A* in the model and determining the percentage of neighboring atoms that belong to each fraction. These percentages are obtained by

$$\eta_{(x)} = 100\frac{\sum_i^{Nx} n_{x,i}}{\sum_i^{Nx} n_{T,i}} \tag{10}$$

where η is the fraction (*Sa*, *R*, or *A*) neighboring the fraction *x* (*Sa*, *R*, or *A*), $n_{x,i}$ is the number of neighboring atoms of atom *i* corresponding to fraction *x*,$n_{T,i}$ is the total number of neighboring atoms of atom *i*, and N_x is the total number of atoms in the model corresponding to fraction *x*. Therefore, in this study, there are three $\eta_{(x)}$ that neighbor the *Sa* fraction ($Sa_{(Sa)}$, $R_{(Sa)}$, and $A_{(Sa)}$), three $\eta_{(x)}$ that neighbor the *R* fraction ($Sa_{(R)}$, $R_{(R)}$, and $A_{(R)}$), and three $\eta_{(x)}$ that neighbor the *A* fraction ($Sa_{(A)}$, $R_{(A)}$, and $A_{(A)}$).

7.3. Ideally homogenous model

An ideally homogeneous model is defined as one whose *Sa*, *R*, and *A* fractions are perfectly mixed, and therefore the composition of the neighboring atoms of every atom in the model is the same regardless of the atom type and position. This means that for the models of bitumen created in this manuscript, composed of

27,656 *Sa* atoms, 12,888 *R* atoms, and 5744 *A* atoms, a perfectly homogeneous mixture is one whose $Sa_{(Sa)}$, $Sa_{(R)}$, and $Sa_{(A)}$ are equal to 59.7%, $R_{(Sa)}$, $R_{(R)}$, and $R_{(A)}$ are equal to 27.8%, and $A_{(Sa)}$, $A_{(R)}$, and $A_{(A)}$ are equal to 12.5%. These will be labelled with the superscript $\eta_{(x)}^{ideal}$ to use as reference throughout the simulations of this study. The value of $\eta_{(x)} - \eta_{(x)}^{ideal}$ is used to evaluate how the arrangement of the SARA fractions compare to those of an ideally homogeneous model of bitumen. If $\eta_{(x)} - \eta_{(x)}^{ideal} \approx 0$, then the model of bitumen is said to be homogeneous at that point in time.

7.4. Regions of interest and potential energy distribution

The *Regions of Interest* are used in all the simulations of this study to track the potential energy of the atoms (see **Equation (5)**) inside these regions and obtain a local distribution of the energies within the models of bitumen throughout the simulations. The local distribution of potential energy is believed to play an essential role in describing the nature of the molecular arrangements that favor phase separation and clustering in MD simulations of bitumen. There are two major regions of interest defined in this manuscript, *interface* regions and *bulk* regions. Algorithmically, an atom is defined to be in an *interface* region if the majority of its *neighboring* atoms belong to a different *Sa*, *R*, or *A* fraction. Meanwhile, it is said to be in a *bulk* region if most of its neighbors belong to the same fraction. The *interface* region is divided into three subregions formed by an interface between asphaltenes and resins (I_{AR}), asphaltenes and saturates and aromatics (I_{ASa}), and resins and saturates and aromatics (I_{RSa}). The *bulk* region is divided into three subregions composed of a bulk of asphaltenes (B_A), resins (B_R), and saturates and aromatics (B_{Sa}). These regions can be visualized in Fig. 6. Molecular rearrangements in homogeneous models are expected to occur due to a high concentration of potential energy in their interface regions[62].

7.5. Interface ratio ($I_{\%}$)

The *interface ratio* is used in parallel to the $\eta_{(x)}$ as a quantitative variable created for this study to categorize bitumen models based on how well (or not) the *Sa*, *R*, and *A* are mixed in the model of bitumen at any given time in the simulation. It measures the ratio of the number of atoms located in an interface region to the total number of atoms in the model, given by

$$I_{\%} = 100\frac{N_I}{N_I + N_B}, \tag{11}$$

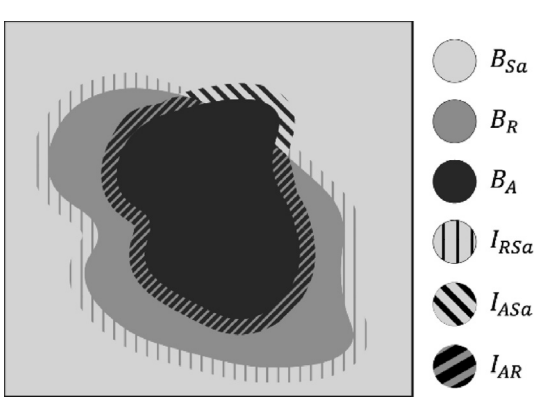

Fig. 6. The *Regions of Interest* consist of *Bulk* regions (B_A, B_R, and B_{SA}) where the atoms are mostly surrounded by other atoms of the same *Sa*, *R*, or *A* fraction, and *Interface* regions (I_{AR}, I_{ASA}, and I_{RSA}), where atoms are surrounded by mostly atoms corresponding to another fraction.

where N_I is the number of atoms in an *interface* region (I_{AR}, I_{ASA}, and I_{RSA}), and N_B is the number of atoms in a *bulk* region (B_A, B_R, and B_{SA}). If the $I_{\%}$ is close to 100%, then most of the atoms are in an interface region, indicating that the model is highly homogeneous, and few distinct molecular arrangements exist in the model. Highly heterogeneous models are expected to have a low $I_{\%}$ because most of the atoms are located inside bulk regions of molecular clusters.

7.6. Asphaltene clusters

Asphaltene molecules are known to show phase behavior and aggregate into molecular clusters several molecules in size. Therefore, a cluster counting algorithm is applied into every step of the simulations to get the number of asphaltene clusters present in a bitumen model at any given time. Algorithmically, an asphaltene molecule belongs to a cluster of asphaltenes if all the carbon atoms of one of its aromatic rings are within neighboring distance of one carbon atom belonging to an aromatic ring of another asphaltene molecule[42]. Single molecules are counted as clusters on their own if there are no other molecules nearby. The latter indicates that for a theoretical mixture of asphaltenes that are perfectly dispersed (where no asphaltene molecule is neighbored by another asphaltene molecule), the number of asphaltene clusters is equal to the number of asphaltene molecules in the model. It is used along the $\eta_{(x)}$ and $I_{\%}$ to formalize the description of the current molecular arrangements in an MD model of bitumen.

7.7. Average volume, volume fraction, and sphericity of asphaltene clusters

The results of the cluster counting algorithm are used to compute the Volume Fraction (V_x), the Average Volume (V_{avg}), and the Sphericity (S_o)[63] of the asphaltene clusters. These quantities help describe the morphology of the asphaltene clusters present in the bitumen models and simulations of this study and aids future researchers in recreating them.

The average volume of each asphaltene clusters is given by

$$V_{\text{avg}} = \frac{\sum_{i=1}^{N_{\text{clusters}}} V_{VdW,i}}{N_{\text{clusters}}}. \tag{12}$$

where $V_{VdW,i}$ is the volume of all the atoms in cluster i using their corresponding Van der Waals radius (R_{ij}^0) and $N_{clusters}$ is the number of asphaltene clusters in the model.

The volume fraction occupied by asphaltenes is given by

$$V_x = \frac{\sum_{i=1}^{N_{\text{clusters}}} V_{VdW,i}}{V}. \tag{13}$$

where V is the volume of the simulation box. The average sphericity of the asphaltene clusters is given by

$$S_o = \frac{1}{N_{clusters}} \frac{\sum_1^{N_{clusters}} \pi^{\frac{1}{3}} (6V_{VdW,\ i})^{\frac{2}{3}}}{S_{VdW,\ i}}, \tag{14}$$

where $S_{VdW,i}$ is the surface area of the $V_{VdW,i}$ region computed using Equation (12) and (13).

7.8. Self-diffusion coefficient

The self-diffusion coefficient (D_{self}) of the molecules is used to track their net movement over time. Computing the D_{self} could aid in indicating if a particular molecular arrangement in the bitumen models can have a considerable impact in their transport properties. This is especially attractive because the D_{self} has been shown to be directly related to more complex quantities, like viscosity or thermal conductivity[64,65]. An overall decrease of

movement in the molecules of the model is expected to occur if the molecular arrangement remains stable over time. The D_{self} is computed using the Stokes-Einstein relation[66]:

$$D_{self} = \frac{1}{6} \lim_{t \to \infty} \frac{d}{dt} \langle (\boldsymbol{r}_n(t) - \boldsymbol{r}_{n,0})^2 \rangle , \quad (15)$$

where D_{self} is the self-diffusivity constant in 3 dimensions, $\boldsymbol{r}_n(t)$ is the position vector of the particles at time t, $\boldsymbol{r}_{n,0}$ is the position of the particles at time t = 0, and the brackets represent the average over the number atoms in the model. D_{self} is continuously computed over 1 ns intervals. In this study, the computed values of D_{self} are compared to those obtained computationally by other researchers, where D_{self}^{lit} equals to 1.0e-11 m^2/s[67,68]. Comparing to experimentally obtained values of D_{self} would be inaccurate because researchers measure D_{self}^{exp} by dissolving specific bitumen fractions in low-viscosity mediums (e.g., dissolving asphaltenes in toluene) at very low concentrations to avoid any display of phase behavior[69,70]. This would mean that D_{self}^{exp} measured using these methods is much larger than those computed using a full bituminous mixture.

8. Results

The following section presents the results obtained from the simulations of the models of bitumen built using both the *Conventional* and *Heterogeneous* methods. For each method, there are two types of result categories: *Bulk* and *Morphological*. *Bulk* results refer to physical, thermodynamic, or transport properties of the models of bitumen in their entirety (e.g., density). *Morphological* results refer to quantities that are related to the local molecular arrangements to formally describe the morphology of a bitumen model (e.g., number of asphaltene clusters).

8.1. Conventional method

8.1.1. Bulk results

8.1.1.1. Density, cohesive energy, heat capacity, and thermal expansion coefficient. Three bitumen models are created using the *Conventional Method*. These are essentially equivalent, with all the three models having the same bulk properties. Table 4 displays a list of the *bulk* properties measured in the relevant points detailed in Fig. 5, including the end of the *Model Construction Method* (points 4 and 5), the first and second *stability runs* (points 6 and 10 respectively), and the *heating cycle* test (points 4–6). The properties in the end of the *Model Construction Method* (point 2) remain stable in all the models, with an average potential energy of 1411.1 kJ/Kg, a T = 298.01 K, and P equal to 1 atm. The density of the models at this stage is similar in every model with an average of ρ equal to 1.008 g/cm^3. This density value compares well to that of bitumen Total 70/100, at ρ = 1.010 g/cm^3 at 298 K and 1 atm. The Cohesive Energy Density (CED) fluctuates between 320 and 331 J/cm^3 between the models, with most of the CED attributed to Van der Waals interactions (99.2%). These compare well to a CED of 311 J/cm^3 and a 99.0% Van der Waal contribution fraction obtained by Xu et Al at these conditions[71]. Therefore, the *Conventional Method* and the MD inputs and simulation parameters (e.g., the PCFF used) effectively produce molecular models that mimic real bituminous materials, at least in terms of properties commonly reported in the literature. Moreover, these properties remain stable until the end of the first *stability run* (point 3), which also implies that the simulation is numerically stable without a thermostat or a barostat. The thermal expansion coefficient (α) and the specific heat capacity (C_p) are obtained from the heating and cooling stages (step 4 through 6), with an α equal to 1.53e-4 1/K at 298 K and 2.38e-4 1/K at 433 K and a C_p equal to 2.11 kJ/kg/K at 298 K and 3.79 kJ/kg/K at 433 K. These values compare well to those found experimentally in previous studies[72] and indicate that the simulation environment is also effective in producing accurate results at higher temperatures. The properties converge again to previous values after cooling back to 298 K and remain stable after the second *stability run* (point 7). Rendered captures of the molecular models produced using the Homogeneous Method are shown in Fig. 7.

8.1.1.2. Potential energy. Even though the difference in the properties of section 8.1.1.1 measured between point 1 and point 7 is too small to draw significant attention, the potential energy of the model is lower by the end of the *Measurement Stage*. The value of E in Point 1 is equal to 1411.1 kJ/kg while in Point 7 is equal to 1375.1 kJ/kg. This suggests that any possible molecular rearrangement is producing a small decrease in the overall potential energy of the model.

8.1.1.3. Self-diffusion coefficient. The calculated values of D_{self} compare well with those found in other studies involving MD simulations of bitumen, both at 298 K and 433 K. At point 2, the D_{self} is equal to 0.811e-11 m^2/s. At point 5, D_{self} is equal to 3.04e-10 m^2/s. The value of D_{self} at point 7 is substantially lower than at point 1 and 2, suggesting that a more heterogeneous molecular arrangement results in a lower net translation of the molecules. A decrease of $\sim$ 20% between Point 1 and Point 7 also indicates that a more stable bitumen morphology can have a substantial impact in the transport properties of a bituminous model, given that the value of D_{self} is key in determining more complex transport properties.

8.1.2. Morphological results

8.1.2.1. Neighboring fractions. The models of bitumen produced using the *Conventional Method* (point 1) have an initial *Sa*, *R*, and *A* fraction distribution that resembles that of an ideally mixed model of bitumen ($\eta_{(x)} - \eta_{(x)}^{ideal} \approx 0$). This can be seen in Fig. 8, where the $\eta_{(x)}$ that neighbor the *Sa* fraction ($Sa_{(Sa)}$, $R_{(Sa)}$, and $A_{(Sa)}$) deviate from ideality at most by 2.5%, the $\eta_{(x)}$ that neighbor the *R* fraction ($Sa_{(R)}$, $R_{(R)}$, and $A_{(R)}$) deviate at most by 4.7%, and the $\eta_{(x)}$ that neighbor the *A* fraction ($Sa_{(A)}$, $R_{(A)}$, and $A_{(A)}$) deviate at most by 5.1%. Nonetheless, the values of $Sa_{(Sa)}$- $Sa_{(Sa)}^{ideal}$, $R_{(R)} - R_{(R)}^{ideal}$, and $A_{(A)} - A_{(A)}^{ideal}$ are the only values that are positive, suggesting that molecules belonging to equal SARA fractions are more likely to be neighbors. By the end of the *Measurement stage* (point 7), the values of $Sa_{(Sa)} - Sa_{(Sa)}^{ideal}$, $R_{(R)} - R_{(R)}^{ideal}$, and $A_{(A)} - A_{(A)}^{ideal}$ increase to 10.4%, 14.5%, and 16.0% respectively, indicating that the grouping of similar fractions occurs in a considerable amount, including both *stability runs* and the *heating cycle*.

Meanwhile, the values of $\eta_{(x)} - \eta_{(x)}^{ideal}$ belonging to different fractions are mostly negative. In the case of the *Sa* fraction, the values of $R_{(Sa)} - R_{(Sa)}^{ideal}$ and the $A_{(Sa)} - A_{(Sa)}^{ideal}$ decrease to −6.8% and −3.5% by the end of the *Measurement* stage, implying that the *Sa* fraction is grouping with itself and pushing both the resins and the asphaltenes away. In the case of the *R* fraction, the value of $Sa_{(R)} - Sa_{(R)}^{ideal}$ decreases to −16.3% while the $A_{(R)} - A_{(R)}^{ideal}$ increases to 2.0%. This indicates that the resins favor being neighbored by resins or asphaltenes instead of saturates or aromatics, at least when considering the initial distribution of neighboring fractions in these particular models. In the case of the *A* fraction, the $Sa_{(A)} - Sa_{(A)}^{ideal}$ decreases to −18%, while the $R_{(A)} - R_{(A)}^{ideal}$ increases to 2.0%. Asphaltene molecules rearrange to strongly separate from saturates or aromatics while favoring being neighbored by resins, a phenomenon that is extensively reported in the literature[74] and

Table 4
List of relevant physical properties and quantitative variables of the model a_1 produced using the *Conventional Method*.

Property	Relevant points in the simulation						
	build		Stab.	Heating cycle			Stab.
	1	2	3	4	5	6	7
Time elap [ns.]	10	40	190	195	205	210	360
$x = y$[Å]	47.64	47.61	47.54	48.88	48.80	47.58	47.59
z[Å]	198.49	198.43	198.39	203.68	203.33	198.26	198.32
T [K]	298	298	298	433	433	298	298
P [atm.]	1.070	1.032	1.002	1.088	1.002	0.948	1.001
ρ[g/cm^3]	1.005	1.006	1.015	0.9303	0.9352	1.009	1.008
α[1/K] ($\cdot 10^4$)	1.53	1.54	1.53	2.37	2.38	1.52	1.52
C_p(kJ/kg/K)	2.11	2.12	2.11	3.81	3.79	2.13	2.10
CED[J/cm^3]	331.78	330.45	325.58	282.77	280.96	324.45	322.02
P_E[kJ/kg]	1411.1	1390.5	1388.0	1721.0	1715.4	1377.3	1375.5
D_{self}[m^2/s] ($\cdot 10^{-11}$)	0.811	0.797	0.763	3.10	3.04	0.767	0.658

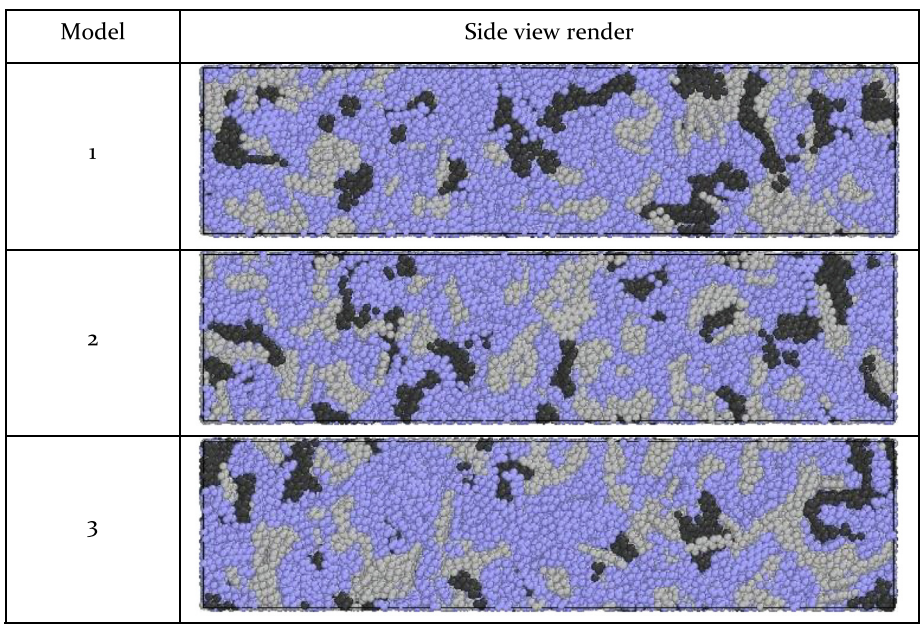

Fig. 7. Side view of the MD models of bitumen built using the *Conventional Method*. The renders are generated using the Open Visualization Tool (OVITO) [73]. The saturates and aromatics (*Sa*) fraction is represented in purple, the resins (*R*) in grey, and the asphaltenes (*A*) in black. (For interpretation of the references to colour in this figure legend, the reader is referred to the web version of this article.)

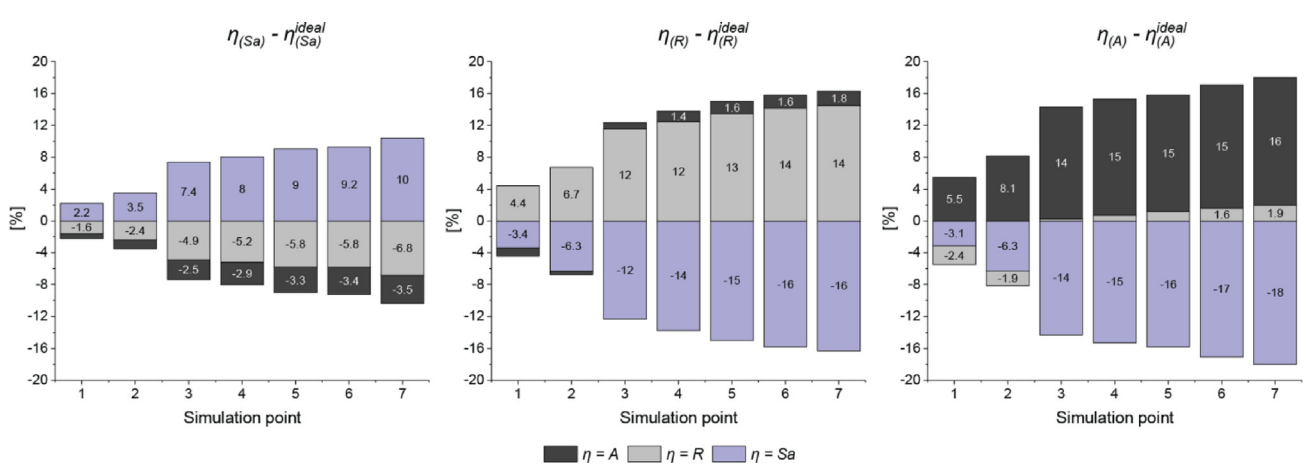

Fig. 8. The subplots show the values of $\eta_{(x)} - \eta^{ideal}_{(x)}$ at different simulations steps for the homogeneous models produced using the *Conventional Method*. The values of $\eta_{(x)} - \eta^{ideal}_{(x)}$ indicate that initially homogeneous models of bitumen undergo a gradual redistribution of molecules that favors the grouping of similar fractions over long simulation times.

one that could be used as evidence to support a colloidal model in bitumens.

The variations of $\eta_{(x)} - \eta_{(x)}^{ideal}$ are more pronounced at the beginning of the *Measurement* stage, even if there is a *heating cycle* aiding in the redistribution process, implying that there could be a molecular arrangement that remains at equilibrium after a certain amount of time. Exposure to higher temperatures during the *heating cycle* allows the molecules to move more freely, overcome local energy barriers, and rearrange to occupy lower energy positions. Intuitively, this suggests that higher temperatures would allow the molecules to mix more thoroughly and produce a more homogeneous arrangement. However, the fraction of *Sa*, *R*, or *A* atoms neighboring other atoms belonging to the same fraction increases steadily over time, even at elevated temperatures. The results also suggest that the models not only evolve to become decreasingly similar to an ideally mixed model of bitumen, but also with respect to the models of bitumen at the beginning of the *Measurement* stage (point 1) (i.e., $\left|\eta_{(x)}^{pointi} - \eta_{(x)}^{point1}\right|$ consistently increases over time).

8.1.2.2. Asphaltene clusters. The number of asphaltene clusters at the beginning of the *Conventional Method* is equal to the number of asphaltene molecules in all the models, where $N_{clusters}$ equal to 48 (each molecule is counted as one cluster). This is the result of evenly distributing all the asphaltenes molecules throughout a low-density simulation box. The V_{avg} of the clusters at this point is equal to 545 A^3 and their S_o is equal to 0.11. The low sphericity value is expected, as asphaltenes molecules are mostly planar. However, in point 1, the number of clusters decreases to 31 clusters, their average volume V_{avg} increases to 1383 A^3, and their sphericity S_o increase to 0.18, indicating that even in early points of the simulations, asphaltene molecules display clustering behavior. With the gradual redistribution of the *Sa*, *R*, and *A* fractions between points 2 to 7 comes a consistent decrease in the $N_{clusters}$ and V_{avg} and an increase in S_o. The $N_{clusters}$ stabilizes by the end second *stability run* (point 7) at an average of 16 clusters, a V_{avg} equal to 2680 A^3, and an S_o equal to 0.27. Their average length spans over 20 Å, still considerably smaller than those suspected to occur experimentally but large enough to be within the lower end of the size domain of colloidal particles. It is evident that clustering is occurring over the course of the simulations. However, more time (or other simulation conditions) are required to accelerate or continue the process. A list of *Morphological* properties can be found in Table 5.

8.1.2.3. Interfacial fraction. These models undergo a gradual, but consistent decrease in the percentage of atoms occupying interfacial regions, which is initially equal to 44.01%, but by the end of the *Measurement* stage it decreases to 37.85%. This suggests that the molecules relocate to occupy regions where they are surrounded by mostly other molecules belonging to the same SARA fraction (i.e., the *Bulk* regions become increasingly larger). The $I_{\%}$ stabilizes throughout the *Measurement* stage, indicating that the model could have reached a morphology comprised of an equilibrated arrangement of its molecules. This behavior has been thoroughly reported in other articles involving the study of mixtures undergoing phase separation[75–77].

8.1.2.4. Potential energy distribution. The gradual rearrangement of the different fractions in the initially homogeneous models of bitumen can be attributed to the local redistribution and gradual decrease of mean potential energies of atoms inside the *Regions of Interest* (seen in Fig. 9).

This indicates that the redistribution process is thermodynamically driven, and results in a molecular arrangement of *Sa*, *R*, and *A* fractions that is energetically more favorable. The mean potential energies of the atoms in all the regions at the beginning of the *Measurement* stage (point 1) are significantly higher to those in the last step (point 7). Certain regions have higher concentrations of mean potential energies when compared to others, even between regions containing molecules of the same fraction. The mean potential energies of the B_R and the I_{SaA} regions are 125.10 kJ/mol/atom and 91.2 kJ/mol/atom, both significantly higher than the mean potential energies of atoms in other regions. The unusually high concentration of potential energy in these regions can be attributed to how the resins are initially artificially placed and therefore misaligned with respect to their amphiphilic poles, and by how asphaltene and saturates and aromatics molecules are known to produce unstable interfaces if there is no stabilizing agent in between. However, these energies decrease steadily with simulation time, and by the end of point 7, the potential energies in the B_R and the I_{SaA} regions are equal to 14.39 kJ/mol/atom and 21.51 kJ/mol/atom respectively. The mean potential energy in the B_{Sa} and B_A regions is considerably lower than in other regions in all the steps of the simulation. This could indicate that molecules in the Sa and the *A* that are beyond interaction range of molecules from other fractions are substantially more stable (their mean potential energy is lower than 4.18 kJ/mol/atom), suggesting that molecules of the same fraction rearrange to minimize the presence of *interfacial* regions. This behavior is ubiquitous in mixtures undergoing phase separation.

Intuitively, the *heating cycle* test results in the increase of the mean potential energies, especially those at the interface. However, by the end of the *heating cycle* (point 6), the mean potential energies are all significantly lower than those at the beginning of the cycle. This means that the *heating cycle* allows molecules to rearrange more thoroughly, escape local energy barriers, and occupy conformations that are ultimately lower in energy. The mean potential energies reach an equilibrium a few nanoseconds into the second *stability run* and remain constant until the end. The halt in the redistribution of energy at the end of the second *stability run* could explain why the *Sa*, *R*, and *A* fractions also stop from rearranging (as seen in Fig. 8), insinuating that the molecular rearrangement of the molecules (and therefore the *Sa*, *R*, and *A* fractions) may have reached a local potential energy equilibrium. The kinetics of the redistribution process (both from *Sa*, *R*, and *A* fractions and the energies) spans over the timescale of tens of nanoseconds (if not hundreds), and the eventual halt in this structural rearrangement does not necessarily mean that the bitumen model has reached an absolute minimum in potential energy. Additional rearrangements may occur if the models are subjected to longer simulation times, to different simulation conditions (e.g., another *heating cycle* step), or to an algorithm that manually relocates individual molecules that actively searches for more energetically favorable conformations (e.g., like those described in Monte Carlo methods).

8.2. Heterogeneous method

8.2.1. Bulk results

8.2.1.1. Density, cohesive energy, heat capacity, and thermal expansion coefficient. Five MD models of bitumen are created using the *Heterogeneous Method*. These are labelled based on the number of asphaltene clusters present at the end of the *Model Construction*, namely a_5, a_4, a_3, a_2, and a_1. For example, a_1 has one asphaltene cluster, and is the most heterogeneous, while a_5 has five asphaltene clusters and is the least heterogeneous. Rendered captures of the molecular models produced using the *Heterogeneous Method* are shown in Fig. 10.

This method is successful in producing bitumen models with stable and realistic bulk properties. It is also effective in producing

Table 5
List of *morphological* properties of the models produced using the *Heterogeneous Method*.

Property	Relevant points in the simulation						
	build		Stab.	Heating cycle			Stab.
	1	2	3	4	5	6	7
Time elap [ns.]	10	40	190	195	205	210	360
$I_{\%}$	44.01	42.17	38.78	38.75	38.41	38.39	37.85
$N_{clusters}$	31	28	22	20	18	17	16
V_{avg}[Å^3]	1383	1532	1949	2144	2382	2523	2680
V_x	0.090	0.089	0.088	0.093	0.094	0.091	0.091
S_o	0.18	0.20	0.25	0.25	0.25	0.25	0.27

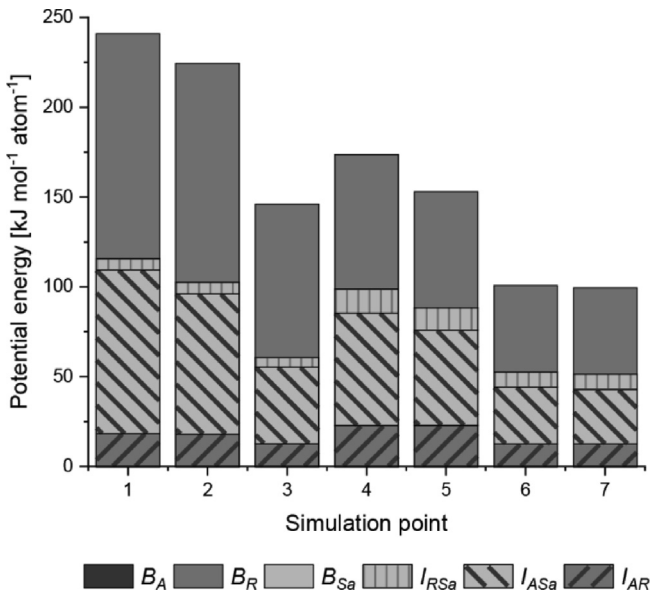

Fig. 9. Potential energy distribution (kJ/mol/atom) in the *Regions of Interest* of the bitumen models produced with the *Conventional Method* throughout the Measurement stage of the simulations.

molecular arrangements similar to those shown in Fig. 4, whose morphologies remain stable even at the end of the *Measurement* stage. The bulk properties of the models (from a_5 to a_1) vary slightly between each other and are comparable to those of the homogeneous models produced with the *Conventional Method*. The density in model a_1 (whose molecular arrangement is the furthest from that of an ideally mixed model and is expected to produce the most pronounced results) by the end of the *stability run* (point 1) is equal to ρ = 1.011 g/cm^3. Its CED is equal to 329 J/cm^3, with most of the CED attributed to Van der Waals interactions (99.4%). Its thermal expansion coefficient (α) and specific heat capacity (C_p) are obtained from the *heating cycle* (step 4 through 6) and are equal to 1.57e-4 m/K at 298 K and 2.35e-4 m/K at 433 K and a C_p equal to 2.14 kJ/kg/K at 298 K and 3.68 kJ/kg/K at 433 K. These properties are essentially equivalent to those found in Table 4, indicating that the density, CED, thermal expansion coefficient, and specific heat capacity are insufficient in effectively determining the impact of having different molecular arrangements. A list of bulk properties of model a_1 is presented in Table 6.

8.2.1.2. Potential energy. The overall potential energy of the model, however, decreases slightly with increasing levels of heterogeneity. The potential energy of model a_5 is 187.29 kJ/kg, 3% lower than in the homogeneous counterparts, while the potential energy of model a_1 is 182.99 kJ/kg, 5% lower than in the homogeneous counterparts. The small difference is not indicative of a definitive preferred molecular arrangement, but it does suggest that the formation of highly heterogeneous arrangements of the order *A-R-Sa* of produce morphologies that are energetically comparable (if not better) than those where all the fractions are homogeneously mixed.

8.2.1.3. Self-diffusion coefficient. The calculated values of D_{self} are substantially lower than the ones computed for the homogeneous models built using the *Conventional Method*. Moreover, they become increasingly smaller with higher heterogeneity. The values of D_{self} for the a_5, a_4, a_3, a_2, and a_1 models at point 3 are equal to 0.557, 0.382, 0.359, 0.336, 0.328 e-11 m^2/s respectively. This indicates that the D_{self} in highly heterogeneous models is around half then one of homogeneous models. Moreover, the difference between the diffusivities in models a_3, a_2, and a_1 is small, suggesting that the value of D_{self} stabilizes beyond a certain degree of heterogeneity in the morphology of the bitumen model. A smaller D_{self} can result in considerably different transport properties. For example, such a decrease can translate into a substantially higher viscosity[64], which could aid in obtaining a better estimate for the viscosity of bitumen, especially when currently published methods to do so underestimate the viscosity by several hundred centipoises.

8.2.2. Morphological results

8.2.2.1. Neighboring fractions. The *Heterogeneous Method* is capable of predictably producing models whose *Sa*, *R*, and *A* fractions are neighbored by an increasing number of molecules belonging to the same fraction. This also means that this method is successful in producing models of bitumen whose *Sa*, *R*, and *A* distributions increasingly deviate away from those of an ideally mixed model of bitumen. This can be seen in Fig. 11, where the $Sa_{(Sa)} - Sa^{ideal}_{(Sa)}$ of models a_5, a_4, a_3, a_2, and a_1 at point 1 deviate from ideality by 18, 22, 28, 32, and 35% respectively, their $R_{(R)} - R^{ideal}_{(R)}$ deviate from ideality by 22, 32, 34, 40, and 46% respectively, and their $A_{(A)} - A^{ideal}_{(A)}$ deviate from ideality by 31, 35, 46, 50, and 56% respectively. Moreover, the molecular rearrangement rate is significantly lower in these models when compared to those of homogeneous models built using the *Conventional Method*. From point 1 through 4, the values of $\eta_{(x)} - \eta^{ideal}_{(x)}$ vary at most by 0.2% (including the $\eta_{(x)}$ values whose η is not equal to the fraction of x), indicating that the neighbor composition of the *Sa*, *R*, and *A* fractions changes negligibly over time, and that the bitumen models are not undergoing a gradual molecular rearrangements like in the case of the bitumen models produced using the *Conventional Method*. The *heating cycle* (points 4 to 6) breaks the stability of the previous stages by pushing the values of $\eta_{(x)}$ to become closer to those of an ideal mixture (by changing them at most by 5%). This means that for the models produced using the *Heterogeneous Method*, a *heating cycle* decreases the values of $Sa_{(Sa)} - Sa^{ideal}_{(Sa)}$, $R_{(Sa)} - R^{ideal}_{(Sa)}$, and $A_{(Sa)} - A^{ideal}_{(Sa)}$, pulling groups of similar fractions apart. Therefore, the *heating cycle* of

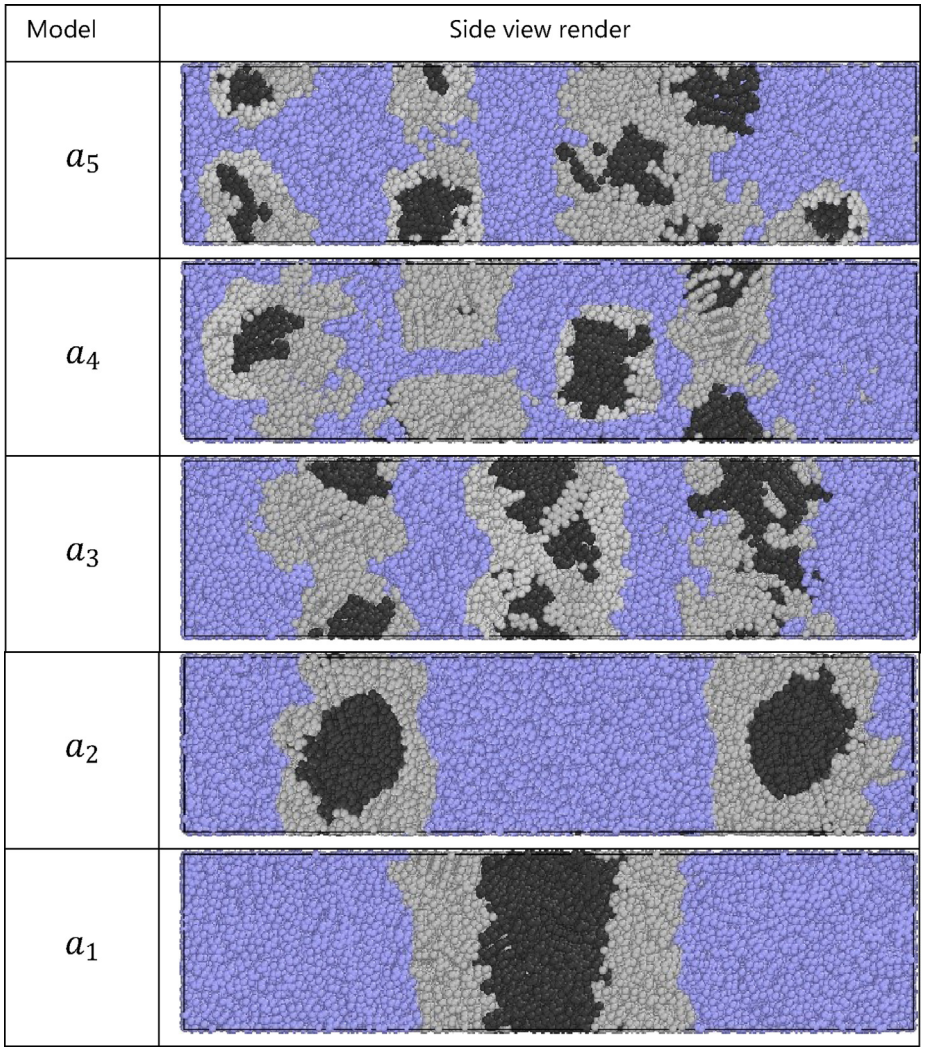

Fig. 10. Side view of the MD models of bitumen built using the *Heterogeneous Method*. The renders are generated using the Open Visualization Tool (OVITO) [73]. The saturates and aromatics (*Sa*) fraction is represented in purple, the resins (*R*) in grey, and the asphaltenes (*A*) in black. (For interpretation of the references to colour in this figure legend, the reader is referred to the web version of this article.)

Table 6
List of *bulk* properties of model a_1 produced using the *Heterogeneous Method*.

Property	Relevant points in the simulation						
	build		Stab.	Heating cycle			Stab.
	1	2	3	4	5	6	7
Time elap [ns.]	10	40	190	195	205	210	360
$x = y$[Å]	47.64	47.61	47.54	48.88	48.80	47.58	47.59
z[Å]	198.17	198.28	198.27	203.30	203.31	198.47	198.11
T [K]	298	298	298	433	433	298	298
P [atm.]	1.054	1.039	0.999	1.082	1.003	0.98	1.001
ρ[g/cm^3]	1.010	1.009	1.008	0.9393	0.9356	1.005	1.010
α[1/K] ($\cdot 10^4$)	1.56	1.54	1.53	2.37	2.38	1.52	1.52
C_p[kJ/kg/K]	2.11	2.12	2.11	3.81	3.79	2.13	2.10
CED[J/cm^3]	338.1	337.8	335.4	274.1	271.9	334.5	333.8
P_E[kJ/kg]	1363	1351	1350	1687	1684	1372	1375
D_{self}[m^2/s] ($\cdot 10^{-11}$)	0.341	0.335	0.328	1.38	1.31	0.345	0.342

Heterogeneous Method has the opposite effect of the *heating cycle* of the *Conventional Method*; an increase in temperature results in certain individual molecules breaking away from the molecular cluster they initially belong to.

8.2.2.2. Asphaltene clusters. The number of asphaltene clusters remains constant throughout the simulations, including both *stability runs* and the *heating cycle* (i.e., points 1 through 7). The number of clusters in models a_5, a_4, a_3, a_2, and a_1 is equal to 5, 4, 3, 2,

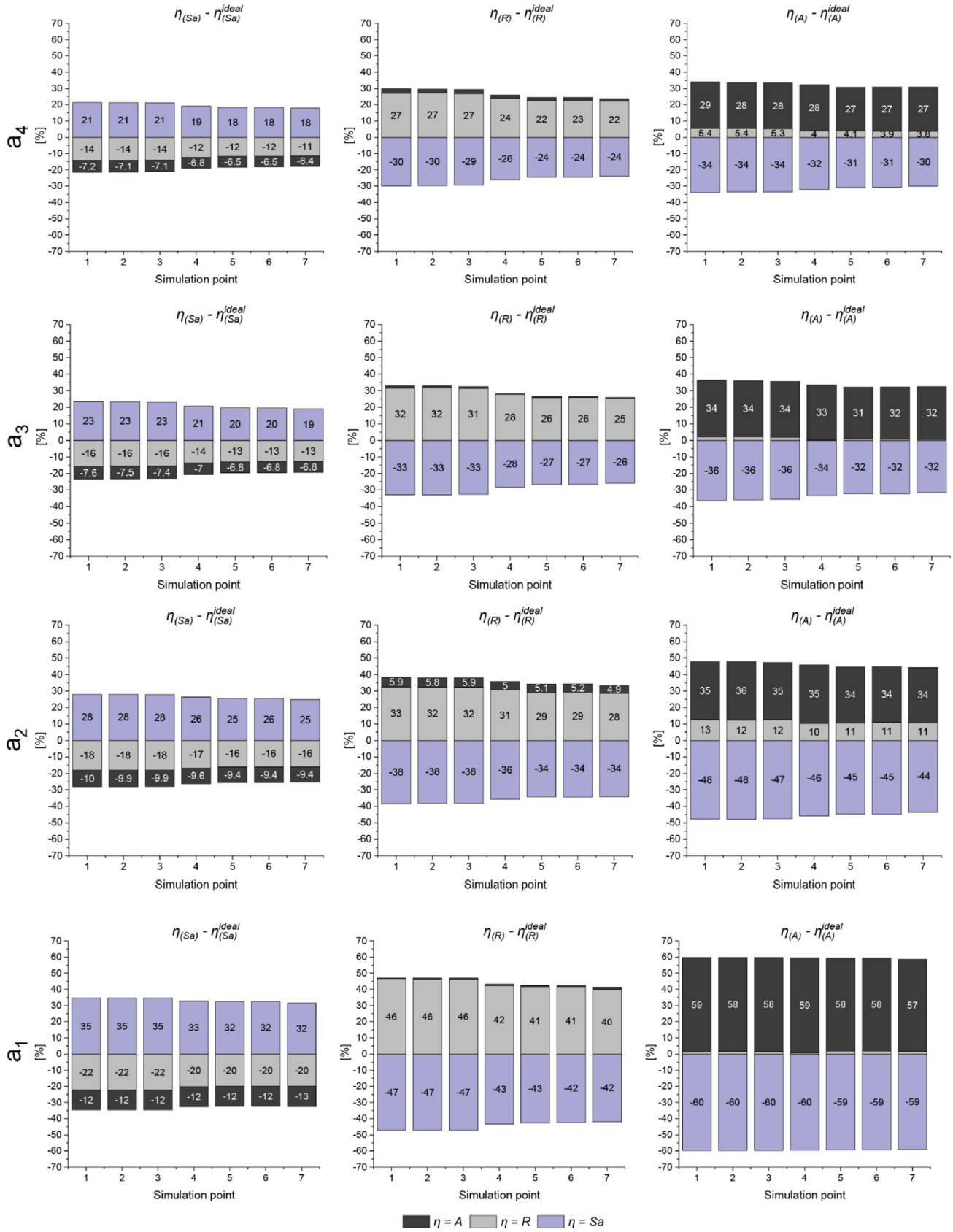

Fig. 11 (*continued*)

and 1 respectively and remain unchanged until the end of the *Measurement stage*. The V_{avg} in models a_5, a_4, a_3, a_2, and a_1 remain constant at 55306, 25881, 17493, 11560, and 9570 Å^3, and the S_o also remain constant at 0.71, 0.91, 0.85, 0.84, and 0.82. Interestingly,

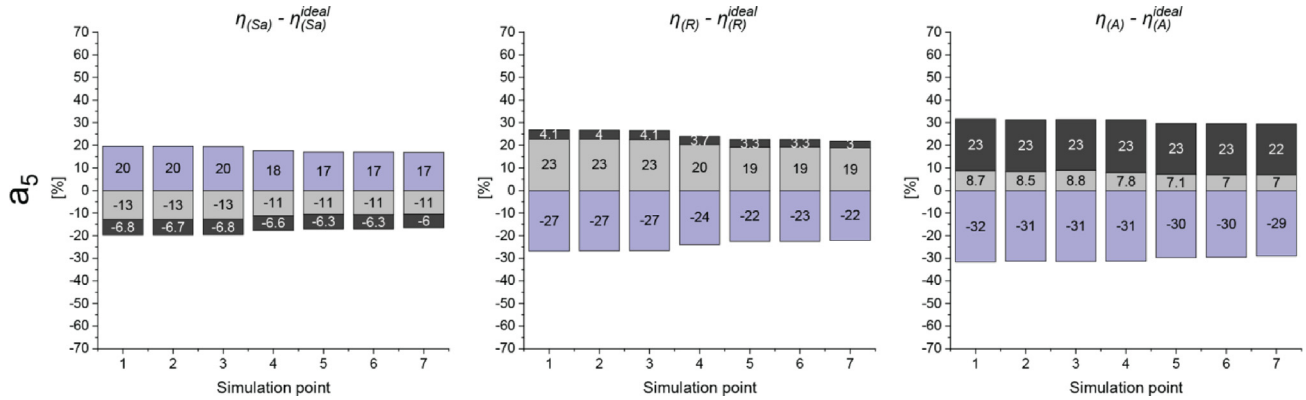

Fig. 11. The subplots show the values of $\eta_{(x)} - \eta^{ideal}_{(x)}$ at different simulations steps. The values of $\eta_{(x)} - \eta^{ideal}_{(x)}$ show that the molecular arrangement in bitumen models built using the *Heterogeneous Method* remains unchanged and is not undergoing rearrangements.

the S_o in model a_1 is not the highest; this could be because the morphology in model a_1 resembles that of a layered model instead of one comprised of spherical arrangements. The negligible variability of these numbers over the course of the simulations indicates that clustering of asphaltene molecules is halted and does not occur in the bitumens produced using the *Heterogeneous Method.* It also implies (given by how the cluster counting algorithm counts a single isolated molecule as a one cluster) that single asphaltene molecules do not separate from the clusters they initially belong to. A list of *Morphological* properties can be found in Table 7.

8.2.2.3. Interfacial fraction. For models a_5, a_4, a_3, a_2, and a_1, the percentage of atoms in an interface region is equal to 27.5%, 25.8%, 20.3%, 15.7%, 6.2% at the beginning of the *Measurement stage* (point 1). This percentage remains stable through point 1 to 3, varying at most by 0.9%. The *heating cycle* (point 4 through 6) increases the values to 30.5%, 28.5%, 22.6%, 17.7%, and 7.9%, which remain stable until the end of the *Measurement stage* (point 7). This suggests that the *heating cycle* is causing the molecules to break out from their initial molecular group, forming new interfacial regions or expanding the size of current ones. This is proven to occur only with molecules of the *Sa* or *R* fractions, as the number of asphaltene clusters remains constant.

The increase in the number atoms occupying interfacial positions also shows how a *heating cycle* has an adverse effect on the molecular arrangement of the *Sa*, *R*, and *A* fractions in a model of bitumen produced using *Heterogeneous Method*. Models that are more homogeneous in nature are impacted the most (given by how the *Sa*, *R* and *A* fractions rearrange, their local potential energies redistribute, and by how the percentage of atoms occupying new interface positions increases the most on these models). This indicates that the shape, size, and arrangement are all important in defining the stability of these features, and that an equilibrium (or optimal) arrangement of the *Sa*, *R*, and *A* fractions may exist in a scale that is still beyond the one simulated in this study.

8.2.2.4. Potential energy distribution. Fig. 12 shows the potential energy distribution of the atoms of models a_5, and a_1 in the *Regions of Interest*. The average potential energies of model a_5 are substantially lower than those of a homogeneous model built using the *Conventional Method* but are considerably higher than those of model a_1 built using the *Heterogeneous Method*. Model a_1 has the lowest average potential energies (from point 1 through 7), suggesting that the models produced using this method result in a more uniform local distribution of energies and that a more heterogeneous morphology (i.e., larger, and more pronounced molecular arrangements) results in all the energies in the *Regions of Interest* to be lower.

The energies of the models from the beginning until the end of the first *stability run* (point 1 to 3) vary at most by 1.2 % (against a 50.5% in the homogeneous models of the *Conventional Method*), which suggests that the energy distribution remains fairly constant over long simulation times and can be used to explain why there is no rearrangement of *Sa*, *R*, and *A* fractions in the bitumens produced using the *Heterogeneous Method*. Interestingly, as the models of bitumen become more heterogeneous (e.g., from models a_3 to a_1), the potential energies of interfacial regions (I_{AR}, I_{ASa}, and I_{RSa}) become negligible or negative. This indicates that the atoms in these regions are in equilibrium or are not being pushed by their surroundings. Such values of potential energies at the interfaces could indicate why there is no thermodynamic incentive for the models to further undergo phase separation. This could also indicate that there exists a set of potential energy values for both *bulk* and *interfacial* regions that produce equilibrated systems (e.g., where all the potential energies become equal).

As expected, the *heating cycle* (steps 4 until 7) increases the overall potential energy values. However, the energies at the end

Table 7
List of *morphological* properties of model a_1 produced using the *Heterogeneous Method*.

Property	Relevant points in the simulation						
	build		Stab.	Heating cycle			Stab.
	1	2	3	4	5	6	7
Time elap [ns.]	10	40	190	195	205	210	360
$I_{\%}$	7.94	8.02	8.00	10.25	10.45	10.53	11.12
$N_{clusters}$	1	1	1	1	1	1	1
V_{avg}[Å^3]	55,778	55,782	55,791	55,812	55,810	55,811	55,764
V_x	0.15	0.14	0.13	0.12	0.12	0.12	0.12
S_o[Å]	0.83	0.83	0.83	0.83	0.83	0.83	0.83

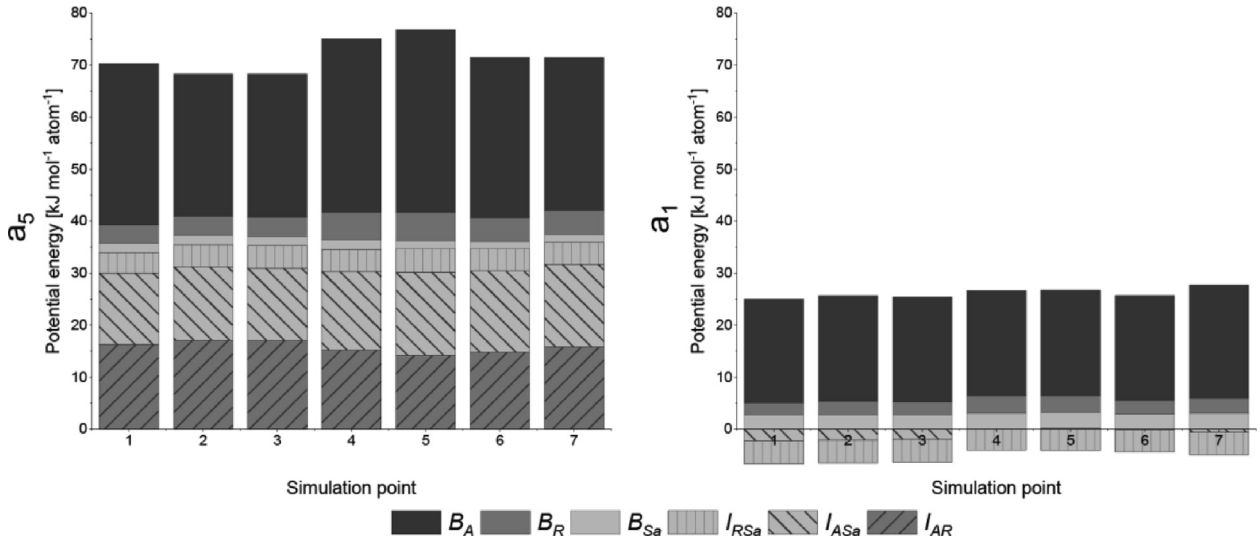

Fig. 12. Potential energy distribution (kJ/mol/atom) in the *Regions of Interest* models a_5 and a_1 produced using the *Heterogeneous Method* throughout the *Measurement stage* of the simulations. The values of the potential energies are considerably lower than those of the *Conventional Method*, especially in the bitumen models with the most heterogeneous structure. The potential energy is almost negligible in the *Interfacial* regions of model a_1, suggesting that interfaces are stable, and explaining why there is no further rearrangement of fractions.

of the *heating cycle* (point 6) do not drop back to their initial levels (point 3) like in those of the *Conventional Method*. These remain higher throughout the rest of the *Measurement Stage*. The increase in energy is more pronounced in models of lower heterogeneity (e.g., a_5) The *heating cycle* has a permanent adverse effect on the energetic stability of the model, especially in the regions that have asphaltenes and resins. This could explain why there are *Sa*, *R*, and *A* fraction rearrangements as shown in Fig. 11, and why there are isolated molecules that break away and diffuse throughout the model. However, the potential energy values in all the *Regions of Interest* still remain considerably smaller than those of the homogeneous models of the *Conventional Method*.

9. Conclusions & future work

The intent of this article focused on studying and implementing the impact of phase separation in MD models of bitumen. This was done as bitumen is known to exhibit phase behavior and is known to display characteristic morphologies that are not accounted for in conventional MD models of bitumen. These are essential in describing it's the behavior of bitumen and in producing a more realistic mechanical and rheological response. This article achieved this by assessing how the SARA fractions and the potential energy are distributed within a model of bitumen, and by showing how these molecules reorganize to form certain arrangements (or morphologies) that result in more favorable energetic configurations over what is currently considered to be a considerably long time in MD. Different bitumen construction methods are also studied to build bitumen models that resemble mixtures that have already undergone phase separation. The results obtained yielded the following conclusions:

(1) Initially homogeneous models of bitumen undergo significant phase separation of its SARA fractions over the course of tens of nanoseconds of simulation time.
(2) The formation of highly heterogenous morphologies whose molecular arrangements resemble those of mixtures that have already undergone significant phase separation is possible in MD models of bitumen. Unlike their homogenous counterparts, these heterogeneous morphologies are highly stable and undergo negligible phase separation over time.
(3) Several physical properties often reported in MD studies of bitumen (e.g., density, cohesive energy density, heat capacity, and thermal conductivity) are equivalent between models of bitumen having different morphologies. More complex techniques (like the ones used in this study) are required to sufficiently assess the impact of different molecular arrangements. Measuring transport properties (e.g., self-diffusion coefficient, viscosity, or thermal conductivity) could be key in differentiating models of bitumen having the same composition, but different morphologies.
(4) Phase separation in MD models of bitumen results in a slightly lower overall potential energy, and in a lower and more even distribution of potential energies between the atoms, especially at the interface between SARA fractions. This indicates that the process is thermodynamically driven, and that the nature of the microstructure in bitumen could be realistically modelled using thermodynamic principles.
(5) A bitumen morphology that results in an absolute minimum in energy is yet to be found. The bitumen models of this study are by no means in perfect equilibrium and are still expected to undergo phase separation if subjected to different conditions. Moreover, a perfectly equilibrated model may still be in a size and time scale that is beyond the ones studied in this article.

The value of this work resides in establishing a set of methods and techniques that will aid scientists in developing more accurate representations of bitumen using MD methods, allowing them to extend their research in:

(1) Implementing large-scale molecular interactions (i.e., phase separation, self-assembly, spinodal decomposition) in MD models of bitumen that are numerically and thermodynamically stable.
(2) Introducing the possibility to directly study the mechanism of formation of different molecular arrangements and morphologies, including those that are characteristic of *Sol* and *Gel* bitumens, using fundamental thermodynamic principles.
(3) Further investigating whether a proper colloidal structure is suitable in describing the nature of the morphology in bitumen.

(4) Developing more complex, but effective techniques to study the impact that different molecular arrangements have on atomistic models of a material having the same chemical composition.
(5) Implement the findings of this study in simulations involving larger size and time scales (e.g., Coarse-grained particle dynamics or finite element methods) to produce more realistic models of bitumen.

Data availability

Data will be made available on request.

Declaration of Competing Interest

The authors declare that they have no known competing financial interests or personal relationships that could have appeared to influence the work reported in this paper.

Acknowledgments

This paper/article is created under the research program Knowledge-based Pavement Engineering (KPE). KPE is a cooperation between Rijkswaterstaat, TNO, and TU Delft in which scientific and applied knowledge is gained about asphalt pavements and which contributes to the aim of Rijkswaterstaat to be completely climate neutral and to work according to the circular principle by 2030. Funding from Rijkswaterstaat is obtained from the grant with case number 31160123 (4th June, 2020). The opinions expressed in these papers are solely from the authors.

Data availability

The raw/processed data required to reproduce these findings cannot be shared at this time as the data also forms part of an ongoing study.

References

[1] D. Lesueur, J.F. Gerard, P. Claudy, J.M. Letoffe, J.P. Planche, D.J.J.o.R. Martin, A structure-related model to describe asphalt linear viscoelasticity, 40(5) (1996) 813-836.
[2] A. Behnood, M. Modiri Gharehveran, Morphology, rheology, and physical properties of polymer-modified asphalt binders, Eur. Polym. J. 112 (2019) 766–791.
[3] D. Lesueur, The colloidal structure of bitumen: Consequences on the rheology and on the mechanisms of bitumen modification, Adv. Colloid Interface Sci. 145 (1) (2009) 42–82.
[4] Z. Yang, X. Zhang, Z. Zhang, B. Zou, Z. Zhu, G. Lu, W. Xu, J. Yu, H. Yu, Effect of aging on chemical and rheological properties of bitumen, Polymers 10 (12) (2018) 1345.
[5] M.L.J.I.J.o.P.E. Greenfield, Molecular modelling and simulation of asphaltenes and bituminous materials, 12(4) (2011) 325-341.
[6] D.D. Li, M.L. Greenfield, Chemical compositions of improved model asphalt systems for molecular simulations, Fuel 115 (2014) 347–356.
[7] F.J.B.M.A. Rostler, Tars, P.N.Y.I. Publishers, Fractional composition: Analytical and functional significance, 2(1) (1965) 151-222.
[8] L.W. Corbett, Composition of asphalt based on generic fractionation, using solvent deasphaltening, elution-adsorption chromatography, and densimetric characterization, Anal. Chem. 41 (4) (1969) 576–579.
[9] G. Leroy, Bitumen analysis by thin layer chromatography (Iatroscan), Proc. 4th Eurobitume Congress, Madrid (1989) 166–170.
[10] A.J.P. Ecker, Coal, The Application of Iastrocan-Technique for Analysis of, Bitumen 43 (1) (2001) 51–53.
[11] A.S.f. Testing, Materials, ASTM D-4124: test methods for separation of asphalt into four fractions, ASTM Philadelphia, 2001.
[12] J.J.T.C. Speight, r.e.M.D.I.N.Y. Technology of Petroleum., Thermal cracking, Chapter 14, (1999) 565-584.
[13] J.A. Koots, J.G.J.F. Speight, Relation of petroleum resins to asphaltenes, 54(3) (1975) 179-184.
[14] J.J.O. Speight, g. science, technology, Petroleum Asphaltenes-Part 1: Asphaltenes, resins and the structure of petroleum, 59(5) (2004) 467-477.
[15] J.F. Branthaver, J. Petersen, R. Robertson, J. Duvall, S. Kim, P. Harnsberger, T. Mill, E. Ensley, F. Barbour, J. Scharbron, Binder characterization and evaluation, Volume 2: Chemistry (1993).
[16] M. Mieczyslaw, M.J.C.o.A. Boduszynski, Advances in Chemistry series, Asphaltenes in petroleum asphalts, 195 (1981) 119-135.
[17] H. Paul Maruska, B.M.J.F.s. Rao, t. international, The role of polar species in the aggregation of asphaltenes, 5(2) (1987) 119-168.
[18] F. Bonemazzi, C.J.J.o.P.S. Giavarini, Engineering, Shifting the bitumen structure from sol to gel, 22(1-3) (1999) 17-24.
[19] C. Giavarini, D. Mastrofini, M. Scarsella, L. Barré, D.J.E. Espinat, Fuels, Macrostructure and rheological properties of chemically modified residues and bitumens, 14(2) (2000) 495-502.
[20] A. Usmani, Asphalt science and technology, CRC Press, 1997.
[21] A.T.J.P.O.P.-A.C.S.D.F.C. Pauli, Asphalt compatibility testing using the automated Heithaus titration test, 41 (1996) 1276-1281.
[22] E.S. Boek, D.S. Yakovlev, T.F.J.E. Headen, Fuels, Quantitative molecular representation of asphaltenes and molecular dynamics simulation of their aggregation, 23(3) (2009) 1209-1219.
[23] Y.J.T.J.o.P.C.A. Ruiz-Morales, HOMO− LUMO gap as an index of molecular size and structure for polycyclic aromatic hydrocarbons (PAHs) and asphaltenes: A theoretical study. I, 106(46) (2002) 11283-11308.
[24] A. Schmets, N. Kringos, A. Scarpas, C. Duif, G. Schitter, T. Pauli, First-principles investigation of the multiple phases in bituminous materials: the case of asphaltene stacking, Advanced Testing and Characterization of Bituminous Materials, Two Volume Set, CRC Press (2009) 159–166.
[25] E. Rogel, L.J.E. Carbognani, fuels, Density estimation of asphaltenes using molecular dynamics simulations, 17(2) (2003) 378-386.
[26] T.F. Headen, E.S. Boek, N.T.J.E. Skipper, Fuels, Evidence for asphaltene nanoaggregation in toluene and heptane from molecular dynamics simulations, 23(3) (2009) 1220-1229.
[27] T.F. Headen, E.S.J.E. Boek, fuels, Molecular dynamics simulations of asphaltene aggregation in supercritical carbon dioxide with and without limonene, 25(2) (2011) 503-508.
[28] D. Frenkel, B. Smit, Understanding molecular simulation: from algorithms to applications, Elsevier, 2001.
[29] F. Alvarez-Ramirez, I. Garcia-Cruz, G. Tavizon, J.J.P.s. Martinez-Magadan, technology, Docking of an asphaltene molecular model on a Fe2O3 surface, an ab initio simulated annealing, 22(7-8) (2004) 915-926.
[30] F. Alvarez-Ramirez, E. Ramirez-Jaramillo, Y.J.E. Ruiz-Morales, Fuels, Calculation of the interaction potential curve between asphaltene− asphaltene, asphaltene− resin, and resin− resin systems using density functional theory, 20(1) (2006) 195-204.
[31] J.S. Hansen, C.A. Lemarchand, E. Nielsen, J.C. Dyre, T.J.T.J.o.c.p. Schrøder, Four-component united-atom model of bitumen, 138(9) (2013) 094508.
[32] X. Qu, Q. Liu, M. Guo, D. Wang, M. Oeser, Study on the effect of aging on physical properties of asphalt binder from a microscale perspective, Constr. Build. Mater. 187 (2018) 718–729.
[33] D.D. Li, M.L. Greenfield, Viscosity, relaxation time, and dynamics within a model asphalt of larger molecules, 140(3) (2014) 034507.
[34] R. Zhai, P.J.R.M. Hao, P. Design, Research on the impact of mineral type and bitumen ageing process on asphalt-mineral adhesion performance based on molecular dynamics simulation method, 22(9) (2021) 2000-2013.
[35] S. Ren, X. Liu, P. Lin, S. Erkens, Y.J.C. Xiao, B. Materials, Chemo-physical characterization and molecular dynamics simulation of long-term aging behaviors of bitumen, 302 (2021) 124437.
[36] X. Ma, J. Wu, Q. Liu, W. Ren, M.J.C. Oeser, B. Materials, Molecular dynamics simulation of the bitumen-aggregate system and the effect of simulation details, 285 (2021) 122886.
[37] Y. Gao, Y. Zhang, Y. Yang, J. Zhang, F.J.A.S.S. Gu, Molecular dynamics investigation of interfacial adhesion between oxidised bitumen and mineral surfaces, 479 (2019) 449-462.
[38] Y. Gao, Y. Zhang, F. Gu, T. Xu, H.J.C. Wang, B. Materials, Impact of minerals and water on bitumen-mineral adhesion and debonding behaviours using molecular dynamics simulations, 171 (2018) 214-222.
[39] D.S. Sholl, J.A. Steckel, Density functional theory: a practical introduction, John Wiley & Sons, 2011.
[40] K. Ohno, K. Esfarjani, Y. Kawazoe, Computational materials science: from ab initio to Monte Carlo methods, Springer, 2018.
[41] P. Carsky, M. Urban, Ab initio calculations: methods and applications in chemistry, Springer Science & Business Media, 2012.
[42] J. Tang, H. Wang, Coarse grained modeling of nanostructure and asphaltene aggregation in asphalt binder using dissipative particle dynamics, Constr. Build. Mater. 314 (2022) 125605.
[43] S. Sengupta, A. Lyulin, Dissipative Particle Dynamics Modeling of Polyelectrolyte Membrane-Water Interfaces, Polymers 12 (4) (2020) 907.
[44] Y. Ruiz-Morales, F. Alvarez-Ramírez, Mesoscale dissipative particle dynamics to investigate oil asphaltenes and sodium naphthenates at the oil− water interface, Energy Fuel 35 (11) (2021) 9294–9311.
[45] Q. Li, J. Cao, Y. Liu, Q. Cheng, C. Liu, Effect of dispersed water on the paraffin crystallization and deposition of emulsified waxy crude oil via dissipative particle dynamics, J. Mol. Liq. 343 (2021) 117679.
[46] D. Guan, S. Feng, L. Zhang, Q. Shi, S. Zhao, C. Xu, Mesoscale simulation for heavy petroleum system using structural unit and dissipative particle dynamics (SU–DPD) frameworks, Energy Fuel 33 (2) (2019) 1049–1060.
[47] F. Alvarez, E. Flores, L. Castro, J. Hernández, A. López, F. Vazquez, Dissipative particle dynamics (DPD) study of crude oil− water emulsions in the presence of a functionalized co-polymer, Energy Fuel 25 (2) (2011) 562–567.

[48] D.H.P.C.C. (DHPC), Delftblue supercomputer (phase 1), (2022).
[49] T. Cosgrove, Colloid science : principles, methods and applications, Wiley, Chichester, West Sussex, 2010.
[50] M.S. Shell, Thermodynamics and statistical mechanics : an integrated approach, (2015).
[51] D.C. Rapaport, The Art of Molecular Dynamics Simulation, 2 ed., Cambridge University Press, Cambridge, 2004.
[52] H. Gould, J. Tobochnik, W. Christian, E. Ayars, An Introduction to Computer Simulation Methods: Applications to Physical Systems, American J. Phys. - AMER J. Phys. 74 (2006) 652–653.
[53] M.G. Paterlini, D.M.J.C.P. Ferguson, Constant temperature simulations using the Langevin equation with velocity Verlet integration, 236(1-3) (1998) 243-252.
[54] S. Weigel, D.J.F. Stephan, The prediction of bitumen properties based on FTIR and multivariate analysis methods, 208 (2017) 655-661.
[55] J.M. Haile, I. Johnston, A.J. Mallinckrodt, S. McKay, Molecular Dynamics Simulation: Elementary Methods, Computers in Physics 7(6) (1993) 625-625.
[56] H. Sun, COMPASS: An ab Initio Force-Field Optimized for Condensed-Phase ApplicationsOverview with Details on Alkane and Benzene Compounds, J. Phys. Chem. B 102 (38) (1998) 7338–7364.
[57] M. Thol, G. Rutkai, R. Span, J. Vrabec, R.J.I.J.o.T. Lustig, Equation of state for the Lennard-Jones truncated and shifted model fluid, 36(1) (2015) 25-43.
[58] B.A. Luty, W.F. van Gunsteren, Calculating Electrostatic Interactions Using the Particle−Particle Particle−Mesh Method with Nonperiodic Long-Range Interactions, J. Phys. Chem. 100 (7) (1996) 2581–2587.
[59] E.M. Blokhuis, D. Bedeaux, C.D. Holcomb, J.A. Zollweg, Tail corrections to the surface tension of a Lennard-Jones liquid-vapour interface, Mol. Phys. 85 (3) (1995) 665–669.
[60] S. Mo, Y. Wang, F. Xiong, C.J.J.o.h.m. Ai, Effects of asphalt source and mixing temperature on the generated asphalt fumes, 371 (2019) 342-351.
[61] F. Ercolessi, A molecular dynamics primer, 2000.
[62] A.R. Van Buuren, S.J. Marrink, H.J. Berendsen, A molecular dynamics study of the decane/water interface, J. Phys. Chem. 97 (36) (1993) 9206–9212.
[63] H. Wadell, Volume, shape, and roundness of quartz particles, J. Geol. 43 (3) (1935) 250–280.
[64] S.H. Jamali, R. Hartkamp, C. Bardas, J. Söhl, T.J.H. Vlugt, O.A. Moultos, Shear Viscosity Computed from the Finite-Size Effects of Self-Diffusivity in Equilibrium Molecular Dynamics, J. Chem. Theory Comput. 14 (11) (2018) 5959–5968.
[65] Y. Zhang, A. Otani, E.J. Maginn, Reliable Viscosity Calculation from Equilibrium Molecular Dynamics Simulations: A Time Decomposition Method, J. Chem. Theory Comput. 11 (8) (2015) 3537–3546.
[66] A. Einstein, Über die von der molekularkinetischen Theorie der Wärme geforderte Bewegung von in ruhenden Flüssigkeiten suspendierten Teilchen, Ann. Phys. 4 (1905).
[67] M. Guo, Y. Tan, L. Wang, Y. Hou, Diffusion of asphaltene, resin, aromatic and saturate components of asphalt on mineral aggregates surface: molecular dynamics simulation, Road Materials and Pavement Design 18 (sup3) (2017) 149–158.
[68] L. You, T. Spyriouni, Q. Dai, Z. You, A. Khanal, Experimental and molecular dynamics simulation study on thermal, transport, and rheological properties of asphalt, Constr. Build. Mater. 265 (2020) 120358.
[69] J.-A. Östlund, M. Nydén, I.H. Auflem, J. Sjöblom, Interactions between Asphaltenes and Naphthenic Acids, Energy Fuel 17 (1) (2003) 113–119.
[70] A.B. Andrews, R.E. Guerra, O.C. Mullins, P.N. Sen, Diffusivity of asphaltene molecules by fluorescence correlation spectroscopy, J Phys Chem A 110 (26) (2006) 8093–8097.
[71] W. Xu, X. Qiu, S. Xiao, G. Hu, F. Wang, J. Yuan, Molecular Dynamic Investigations on the Adhesion Behaviors of Asphalt Mastic-Aggregate, Interface 13 (22) (2020) 5061.
[72] W.R. Lindberg, R.R. Thomas, R.J. Christensen, Measurements of specific heat, thermal conductivity and thermal diffusivity of Utah tar sands, Fuel 64 (1) (1985) 80–85.
[73] A. Stukowski, Visualization and analysis of atomistic simulation data with OVITO–the Open Visualization Tool, Model. Simul. Mater. Sci. Eng. 18 (1) (2009) 015012.
[74] Y. Zhang, M. Siskin, M.R. Gray, C.C. Walters, R.P. Rodgers, Mechanisms of Asphaltene Aggregation: Puzzles and a New Hypothesis, Energy Fuel 34 (8) (2020) 9094–9107.
[75] S. Koch, R.C. Desai, F.F. Abraham, Dynamics of phase separation in two-dimensional fluids: spinodal decomposition, Phys. Rev. A 27 (4) (1983) 2152.
[76] K. Elder, T. Rogers, R.C. Desai, Early stages of spinodal decomposition for the Cahn-Hilliard-Cook model of phase separation, Phys. Rev. B 38 (7) (1988) 4725.
[77] E. Favvas, A.C. Mitropoulos, What is spinodal decomposition, J. Eng. Sci. Technol. Rev 1 (1) (2008) 25–27.